Appendix D - Calculation report Xmas Tree Handling Tool (XTHT), 70 tonnes

Abstract

This calculation report intends to prove the structural integrity and confirm the 70 tonnes lifting capacity of the Xmas Tree Handling Tool (XTHT), in both a center and off-center lifting position. The analysis basis is described, followed by Finite Element Analysis (FEA) and hand calculations to reach the objectives. Based on the results and discussions, the XTHT was concluded to have sufficient strength, but needs to be controlled and verified by professionals. A list of further work which is necessary before any implementation was also made.

Contents

List of Figures

List of Tables

Acronyms

COG Center Of Gravity. 65

DOF Degree Of Freedom. 18

FEA Finite Element Analysis. i, 2, 4, 13, 72

WLL Working Load Limit. 5

XT Xmas Tree. 5, 10, 55

XTHT Xmas Tree Handling Tool. i, 1, 4, 10, 37, 55, 66, 72

1 Introduction

The Xmas Tree Handling Tool (XTHT) performs lifting and handling of subsea Xmas Trees. The tool has an adjustable lifting point and can perform lift which is displaced from the spool center. The tool needs to have sufficient strength to perform the intended lifting operations, both in a center and off-center position. The objective of this report is to verify structural integrity of the tool and confirm its 70 tonnes lifting capacity. Worst case scenarios are also taken into account. The report is carried out in accordance with the requirements stated in the "Design basis" (appendix A) and it structured in such a way that the results can be verified or reproduced.

2 Theory

2.1 Finite element analysis

Siemens NX Finite Element Analysis (FEA) application is used throughout the calculation report as a computer assisted calculation tool. This application allows the designer to perform structural or performance analysis of a product or a system in a virtual environment. The purpose is to solve a potential and uncertain issues or cases[1]. For example, this analysis could be used to predict how a 3D model would respond to stress or other environmental factors.

Note: Basic knowledge of the Siemens NX software and its FEA application is an advantage and will ease the reading of the report.

2.2 Hooke's law

The calculation is based on having elastic deformation of the steel. The theory of Hooke's law applies to this and express the relationship between stress and change of shape. Hooke's law is stated:

$$\sigma = E * \varepsilon$$

The law shows that the tension(σ) is proportional to the strain (relative extension, ε). The law could be derived by applying load to a bar of steel and thereby measure the extension. The Young's modulus (E) is a constant which is equal to the theoretical tension required to elastically extend the steel bar with 100%. Thereby, Young's modulus indicates the stiffness of the material [2]. Figure 1 shows the result of such an experience. Note that in the FEA, a linear solver has been.

The result is a typical stress-strain diagram of steel. Hooke's law and elastic deformation no longer applies as the tension reach the yield stress of the material, as the diagram shows. Any further loads will result in plastic deformation or dislocation slip in the material, where the atomic plane in the lattice of crystalline materials slips and translates a long their direction. This results in a permanent change of shape [2].

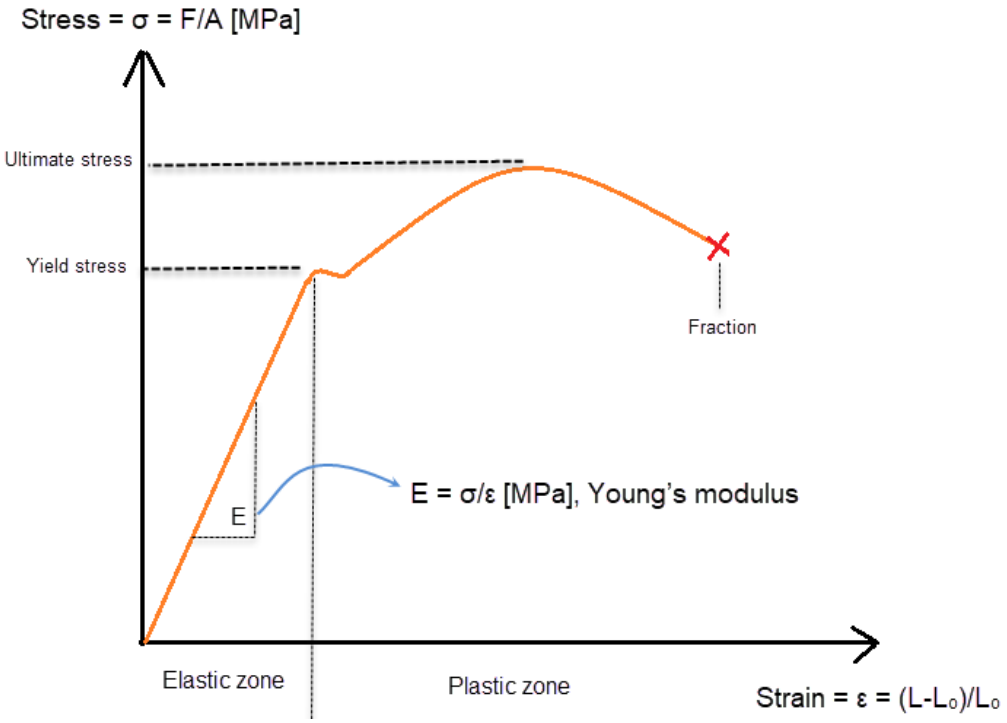

Figure 1: Typical Stress - Strain curve for steel

3 Method

This chapter covers all calculations done to confirm the 70 tonnes lifting capacity of the XTHT. The chapter is separated into the following sections.

- **Calculations and analysis basis**
- **Finite Element Analysis**
- **Hand calculations**

3.1 Calculations and analysis basis

This section covers the information and basis which is necessary to carry out the calculations, such as tool geometry, load description and material properties.

3.1.1 Method and tool geometry

Every part of the tool that experience or generate any load is calculated separately. Separately calculations is done due to lack of competence in contact FE simulations and therefore would separately calculations be the most time efficient approach. Forces and constrain is settled in a way that corresponds to load path shown in the next section and thereby the results would be approximately equal to a contact simulation.

The calculations includes both hand calculations and Finite Element Analysis (FEA). Independently of the method, the calculations verifies structural integrity of each single part and together verify structural integrity of the whole tool. Figure 2 and Table 1 shows the geometry and describes the different components which is analyzed.

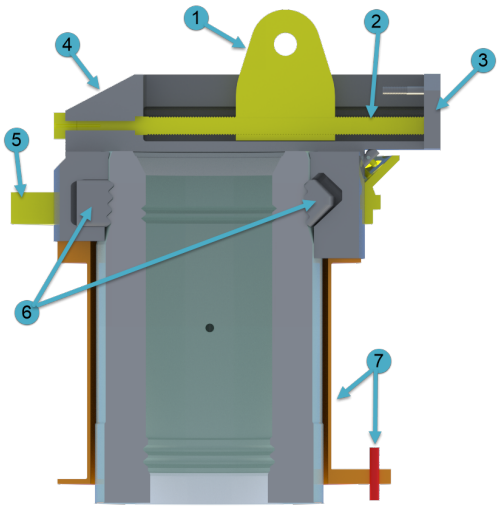

Figure 2: Section view of the XTHT

Number	Description	Method
1	Lifiting lug	FEA
2	Screw	Hand
3	End cap	Hand/FEA
4	Main body	FEA
5	Locking ring	FEA
6	Locking dogs	FEA
7	Funnel and pin	Hand/FEA

Table 1: Component overview

3.1.2 Load description

The calculations is performed as static load scenes, with the lifting load as the only load that relates to the tool. The only lifting load case would be a vertical lift of the XT. However, the tool will experience different load cases due to it's adjustable lifting point. Therefore, two lifting cases are taken into account during the calculations, which are as follows:

- Center lift
- Max Off-center lift

Note: It is worth to mention that center is defined as the center of the cylindrical spool.

Note: Misalignment of the tool introduces new load cases. This is covered along.

The Working Load Limit (WLL) for the lifting operations is at 70 tonnes. But due to the safety factor, which is covered in appendix A, the applied design load is at 280 tonnes. This makes an applied force at:

$$F = 280t * 1000\frac{kg}{t} * 10\frac{m}{s^2} = 2'800'000N$$

The gravitational acceleration coefficient i settled to $g = 10\frac{m}{s^2}$ instead of $g = 9.81\frac{m}{s^2}$. This is done due to the uncertainty of the tool's weight. The final weight of the tool is not settled in this phase of the bachelor thesis, as components that does not take any loads could be added later on. Using $g = 9.81\frac{m}{s^2}$ results in an applied force at $F = 2746800N$. Compared to using $g = 10\frac{m}{s^2}$, the force is $53200N$ lower, which is equivalent to approximately 5.4 tonnes. appendix A - "Design basis", gives a maximum tool weight at 5 tonnes and thereby is $g = 10\frac{m}{s^2}$ a conservative and safe value, as well as the number is easier to use.

Figure 3 shows the load path through the tool as is locked to the H4 profile and lifted from the shackle. The red arrow illustrates the force that the locking ring needs to withstand. This horizontal force is generated by the angled support face in the "locking dog - H4 profile" interface.

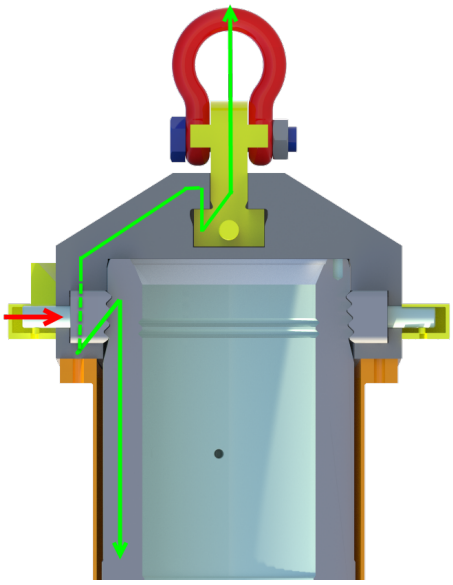

Figure 3: Load path through the tool

Figure 4 and Figure 5 illustrates how the load path changes during a off center lift.

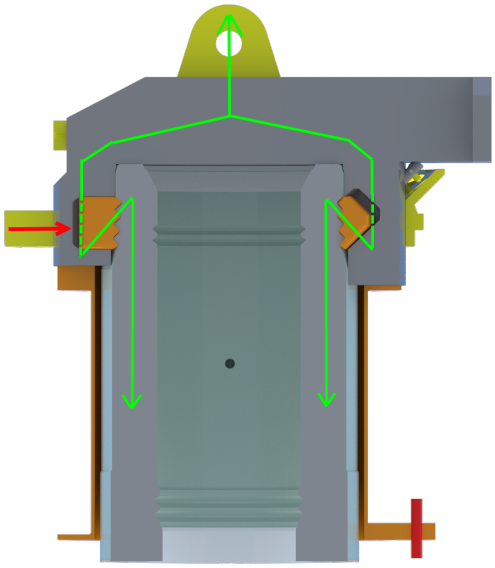

Figure 4: Load path during a center lift

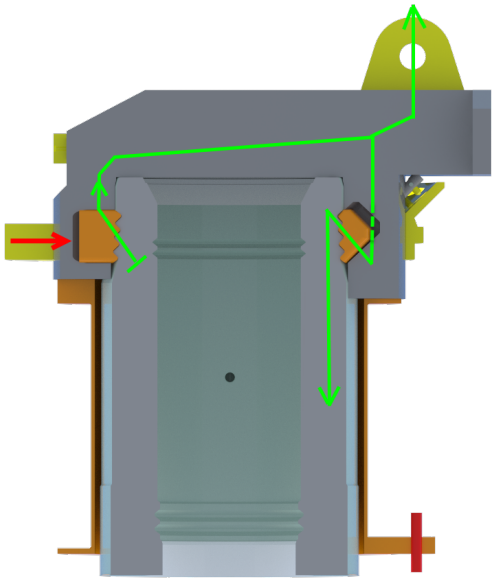

Figure 5: Load path during a off-center lift

As Figure 5 illustrate, the load paths changes direction on the left side of the tool when the lift point is located off-center. Off-center lifting introducing extra loads to the dogs closest to the lifting point, as they need to withstand the upward load at the leftist locking dogs to achieve equilibrium. The load increases along with the increased off-center distance, where the maximum off-center distance is at 0.5m, referring to appendix A. This effect would be referred to as "the bottle opener effect".

To ease the reading, this section reflects the load that every component will experience during a center lift or a off-center lift. The components is shown in the previous section. Throughout the calculation report, the force values will only be mentioned, sourcing this section.

Only the following components will experience loads during a center or an off-center lift:

- Lifting lug
- Main body
- Locking dogs
- Locking ring

Note: This requires that the tool is correctly aligned. Otherwise, the XT would tilt and introduce new load cases. These are listed at the end of this section.

The lifting lug and main body interface will have a load case were both components experience the lifting force at 2800kN, independently of the position of the lifting lug.

However, the forces acting at the locking dogs various along with the lifting lug off-center position, as Figure 4 and 5 shows. The following calculations shows the forces acting in the locking dogs/locking dog housings.

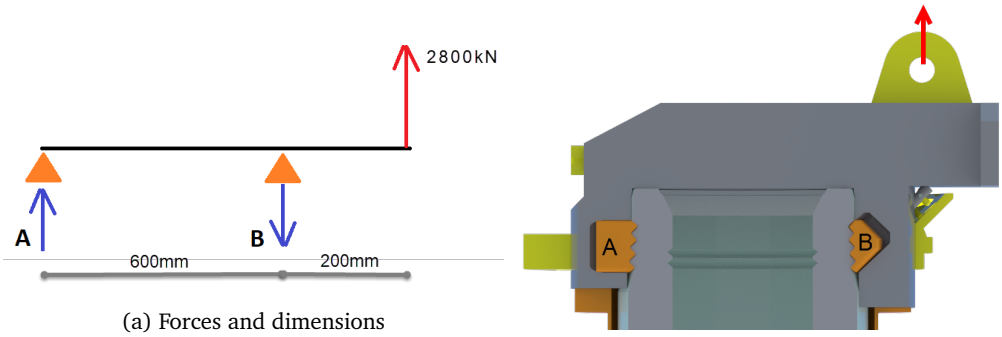

(a) Forces and dimensions

(b) A and B location

Figure 6: Force and dimension overview - Off-center lift

$$\Sigma M_A = 0 \Rightarrow F_B * 600mm - 2800kN * 800mm = 0$$

$$\Downarrow$$

$$F_B = \frac{2800kN * 800mm}{600mm} = 3733kN$$

$$\Sigma F = 0 \Rightarrow -2800kN + F_B - F_A = 0$$

$$\Downarrow$$

$$F_A = F_B - 2800kN = 3733kN - 2800kN = 933kN$$

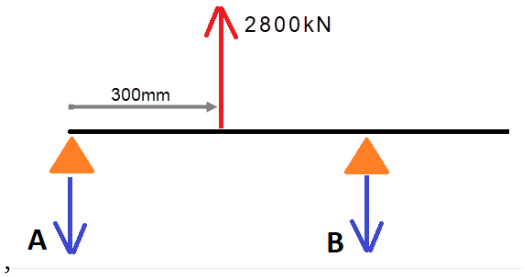

Figure 7: Force and dimension overview - Center lift

Center positioned lifting force ⇓

$$F_A = F_B = \frac{2800kN}{2} = 1400kN$$

The calculations above reflects how the forces distributes at each side of the tool, in a two-dimensional view. However, the tool is equipped with a total of six locking dog. Figure 8 shows this, while the following itemization reflects the force distribution to the dogs.

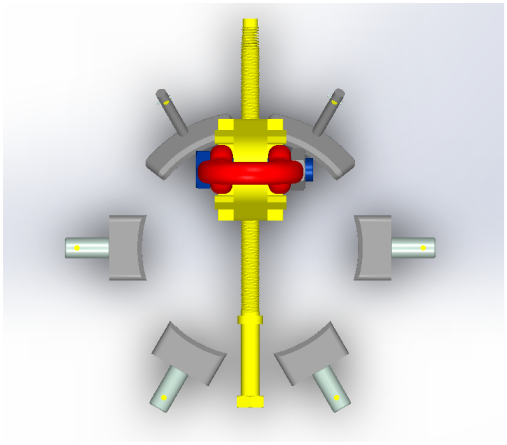

(a) First view

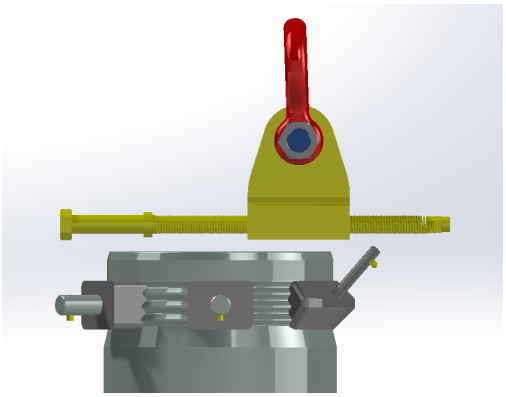

(b) Second view

Figure 8: All six locking dogs

- **Center lift**
  Each dog would experience a upwards load at $F = \frac{2800kN}{6} = 467kN \Rightarrow F = 470kN$.
- **Off-center lift**
  The load distribution in the off-center scenario is difficult to calculate in this phase of the product development. It depends on tolerances in the locking dogs interfaces, which are not yet settled.
  Therefore, a simplification was done, were the two middle dogs does not experience any load. This is considered as the most sufficient and correct approach at this time of the development. Thereby, two locking dogs at the "A side" and two locking dogs at the "B side" would experience load, which are as follows:
  - Force per dog at "A-side": $F_A = \frac{933kN}{2} = 467kN \Rightarrow F_A = 470kN$
  - Force per dog at "B-side": $F_B = \frac{3733kN}{2} = 1867kN \Rightarrow F_B = 1870kN$

"A-side"	"B-side"
Load description The H4-profile has an angled locking profile at 45°. The angled interface generates a greater normal force in the locking profile. Decomposing this provides the horizontal force which the transmission pin transfer into the locking ring.	**Load description** As mentioned in the left column, the angled interface generates a higher normal force. The support surface of the locking dogs in the main body is angled by 45°. This results in no loads at the locking ring at the B-side, as the main body repeals the normal force by it self.
Center lift Force acting on straight locking dog: $F = \frac{470kN}{\cos 45°} = 665kN$ Force acting in the locking dog housing: $F = 470kN$ Force acting on transmission pin: $F = 665kN * \sin 45° = 470kN$	**Center-lift** Force acting on tilted locking dog and its housing in the main body: $F = \frac{470kN}{\cos 45°} = 665kN$
Max off-center lift Force acting on straight locking dog: $F = \frac{470kN}{\cos 45°} = 665kN$ Force acting in the locking dog housing: $F = 470kN$ Force acting on transmission pin: $F = 470kN$ *Note: The forces acts in the opposite direction, as shown in Figure 5.*	**Max off-center lift** Force acting on tilted locking dog and its housing in the main body: $F = \frac{1870kN}{\cos 45°} = 2640kN$

Table 2: Load calculations of forces in locking dog interfaces, related to Figure 9.

(a) A-side (b) B-side

Figure 9: Force overview in locking dog interfaces

Table 3 shows and overview of the forces which is going to be applied to the different components during the calculations.

Force to be applied in the calculations [kN]

Component	Center lift			Max off-center lift	
Lifting lug	2800			2800	
Main body, upper part	2800			2800	
Main body, locking dog housings	A-side	Middle	B-side	A-side	B-side
	470	470	665	470	2640
Straight locking dog	665			665	
Tilted locking dog	665			2640	
Locking ring	470			470	

Table 3: Force overview

There are two extraordinary load cases which are not explained in this section, which are as follows:

1. **Tilted lift of the XT**
   Lifting with a tilt introducing new forces to the XTHT and creates new load cases. This load case is covered in section 3.2.11 - "FE analysis no. 10".
2. **Preventing rotation of the XTHT at the spool**
   During a misalignment of the XTHT, a torque would be generated. The anti-rotation withstands this and prevent any possible rotation. This introducing loads to both the anti-rotation pin and the funnel. This load case is covered in section 3.2.10 - "FE analysis no.9".

3.1.3 Material data

This section shows which material present for the differente components. Based on appendix A - "Design basis", the main material to be used is AISI 8630 MOD 80ksi, alloyed steel. However, it also states that other material could be used if its beneficial. Table 4 shows the chosen material at the different components.

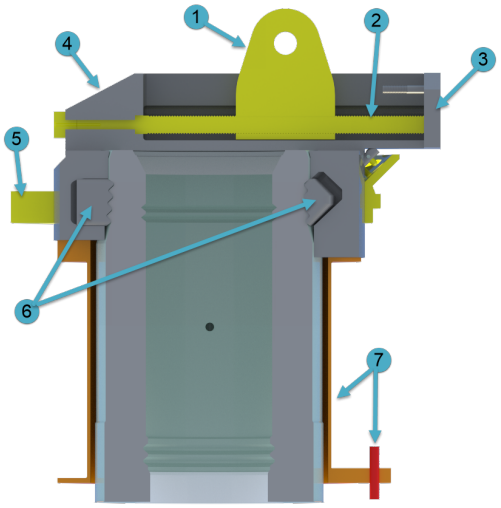

Figure 10: Section view of the XTHT

No.	Description	Method
1	Lifiting lug	AISI 8630 80ksi
2	Screw	TTSTE 355 Z3
3	End cap	AISI 8630 80ksi
4	Main body	AISI 8630 80ksi
5	Locking ring	AISI 8630 80ksi
6	Locking dogs	AISI 8630 80ksi
7	Funnel	TTSTE 355 Z3
7	Anti-rotation pin	TTSTE 355 Z3
N/A	Transmission pin	AISI 8630 80ksi
N/A	Brackets (anti-rot.)	TTSTE 355 Z3
N/A	End cap bolts	TTSTE 355 Z3

Table 4: Material of the different components

Figure 11 shows an overview of different materials used in Aker Solutions, including AISI 8630 80ksi and TTSTE 355 Z3. The diagram reflects when plastic deformation occurs to the different materials.

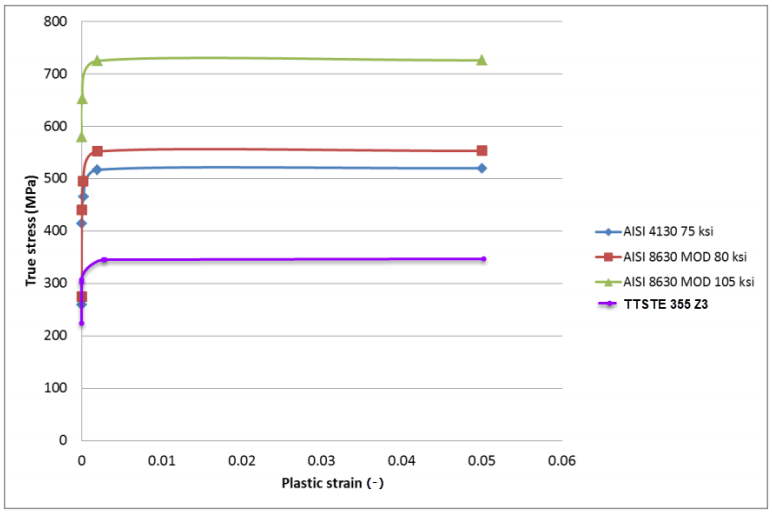

Figure 11: Stress - Strain curves for familiar materials in the company (Source: Aker Solutions)

Table 5 shows the material properties of AISI 8630 MOD 80ksi and TTSTE 355 Z3 [3].

Properties	**AISI 8630 MOD 80ksi**	**TTSTE 355 Z3**	**Unit**
Young's modulus, E	191 300 (27 750)	200 350 (29 058)	Mpa (ksi)
Poisson' s ratio, ν	0.3	0.31	(-)
Yield Stress, σ_y	552 (80)	355 (52)	MPa (ksi)
Ultimate Tensile Stress, σ_u	689 (100)	460 (67)	MPa (ksi)

Table 5: Material properties

3.1.4 Acceptance criteria

Stress

The calculation is based on having elastic deformation of the material. Hooke's law then applies to the calculations, referring to chapter 2 - "Theory". Plastic deformation resulting in a permanent change of shape is not acceptable.

$$\sigma = \frac{F}{A} = E * \varepsilon$$

The yield stress for AISI 8630 is at $\sigma = 552MPa$ and $\sigma = 355MPa$ for TTSTE 355 Z3, referring to Table 5. These are the maximum tensions before plastic deformation occurs and will therefore be the maximum accepted stress in the calculations. Due to the safety factor, the applied force would be at $F = 2800KN$, as mentioned in section 3.1.2.

Displacement

Displacement of the material would occur along with the elastic deformation, as Figure1 shows. Determining a certain and general value as displacement a would be inexpedient. Acceptable displacement of the material would be situational, depending on how crucial the displacement is. Therefore, every maximum displacement would be discussed and evaluated were this is analysed. This was concluded during a meeting, see appendix J - statusmeeting sverre 150419

3.1.5 Conservative factors

This subsection list some factors that contribute to conservative and more reliable analysis. The factors are common for all the analysis throughout the report.

- **Gravitational acceleration coefficient**
  Settled to $g = 10\frac{m}{s^2}$ instead of $g = 9.81\frac{m}{s^2}$, see section 3.1.2.
- **Friction**
  All friction that reduces applied force has been neglected.
- **Safety factor**
  The safety factor is 3.99. In this calculation report, 4 has been used.

3.2 Finite Element Analysis

This section covers Finite Element Analysis (FEA) of all components where hand calculations is too challenging. Table 3.1.3 gives an overview of the analysis.

The first component in the description shows which component that is analyzed, while the second addresses the component that interferes. Every analysis is described and structure with following subsections:

1. Geometry
2. Mesh
3. Boundary conditions
4. Result and discussion

FE Analyzes

No.	Description
1	Lifting lug - Main body
2	Main body - Lifting lug. Off-center lift
3	Main body - Lifting lug. Center lift
4	Main body - Locking dogs. Off-center lift
5	Main body - Locking dogs. Center lift
6	Locking dog - Main body. Straight locking dog
7	Locking dog - Main body. Tilted locking dog
8	Locking ring - Transmission pin
9	Funnel - Anti-rotation pin
10	End cap - Screw

Table 6: Overview of the analyzes

The component of every analysis is applied with the applicable material, referring to section 3.1.3 - "Material data"

When performing FEA in Siemens NX, Nastran SOL 101 has been used as a solver

3.2.1 Siemens NX commands and mesh properties

This section covers a basic explanation and usage intentions of difference Siemens NX commands and mesh properties, used to make and mesh the FE models throughout the analysis.

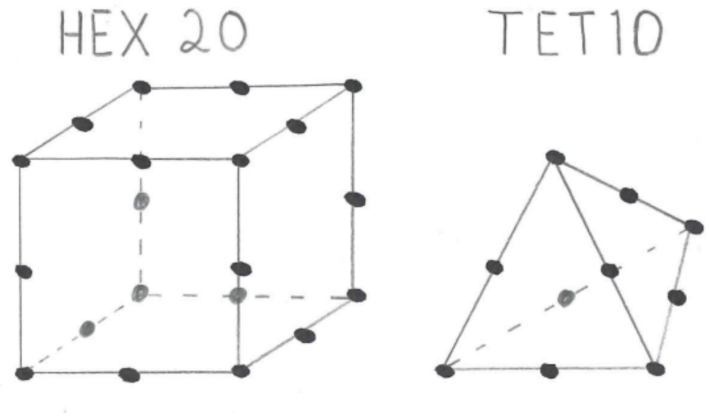

Figure 12: Element Types. The dots represent nodes

- **HEX20 elements**
  HEX20 is a square element with 20 nodes. These are the preferred elements since they deliver more accurate results that TET does.
- **TET10 elements**
  TET10 is a triangular pyramid element with 10 nodes. These elements adapts better to curves and uneven geometry, the down side is that they are not as accurate as HEX elements.
- **Split body command**
  You need a straight, uniform body if you want to apply a HEX mesh. By using the split body command the model can be split into several individual uniform bodies which can be applied a HEX mesh.
- **3D swept mesh**
  When the body has a uniform geometry, a HEX mesh can be applied. By the use of the "3D swept mesh" command a body can be meshed by sweeping a 2D mesh across a uniform body.
- **Mesh mating command**
  When the body is split and all the individual bodies are meshed, mesh mating needs to be done to be able to run the simulation. The mesh mating command make sure that all of the individual meshes is connected properly so the model appears as one.
- **Mesh density**
  Solving a FEM analysis can be time consuming. The finer the mesh, the more accurate result, the more time consuming analysis. The trick is to have a fine mesh in critical areas with stress concentration, and a course mesh elsewhere. The mesh density command is used to achieve this.

3.2.2 FE analysis no. 1: Lifting lug - Main body

This analysis covers the lifting lug, analyzing the load transfer between the lifting lug and the main body.

Geometry

The geometry of the lifting lug is shown in Figure 13. Notice the coordinate system.

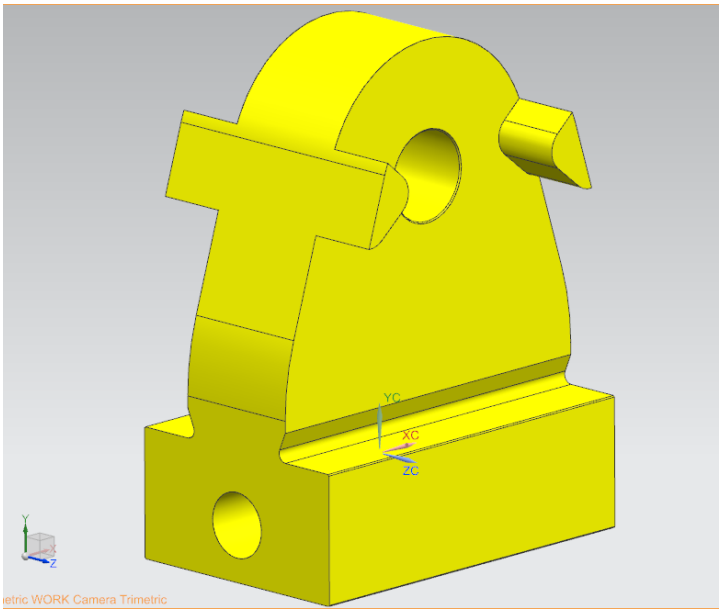

Figure 13: Lifting lug geometry

The lifting lug is symmetric in both the ZY- and XY plane. Therefore, a symmetric FE model is made to ease the computational process, shown in Figure 14. This allows for a higher mesh concentration in critical areas, which in this case is the curvature.

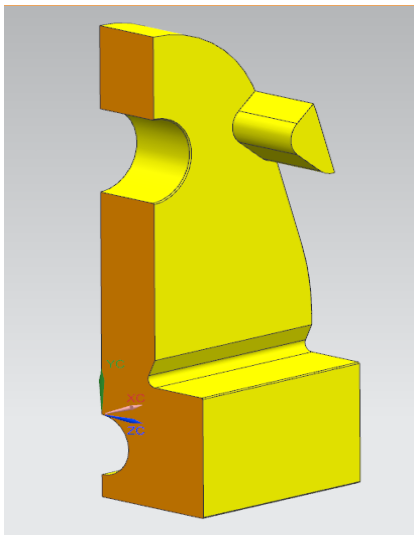

Figure 14: FE model - Lifting lug

Mesh

Table 7 and Table 8 covers the mesh strategy and the mesh result, respectively. The following figures shows the finished mesh.

Meshing data

Strategy	**Element**		**Features**
	Type	Size	Split body.
The FE model is split into several bodies and meshed with HEX20 and TET10 elements, where HEX20 was applied to the most critical area. In this case, the critical area is at the curvature. HEX20 is also applied to two additional surfaces, which is clearly shown in Figure 15a. The mesh density at the shackle hole is set to 4mm. This is due to the constrain that will be applied to the hole (next section).	HEX20	2mm	Mesh mating command.
	TET10	40mm	3D Swept mesh.
			3D Tetrahedral mesh.
			Mesh control.

Table 7: FE analysis no.1 - Mesh strategy

Mesh result

Number of elements	Number of nodes
HEX20: 986 TET10: 63567	95663

Table 8: FE analysis no.1 - Mesh result

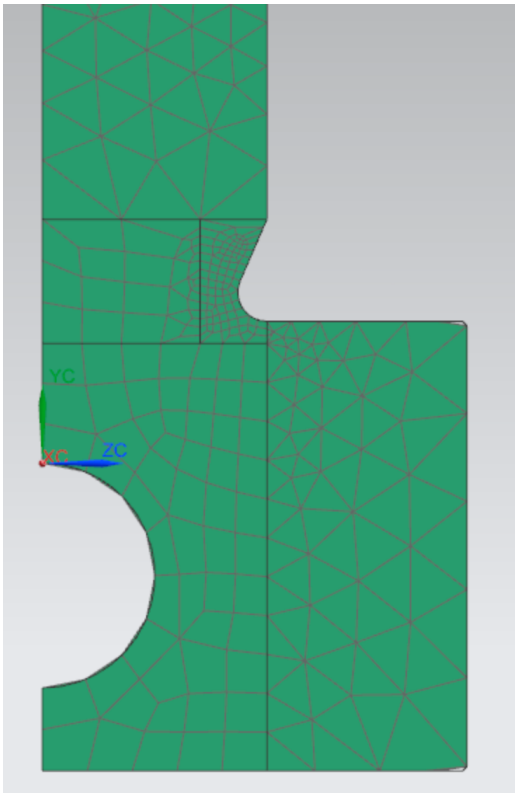

(a) Figure shows the 2D surfaces were the HEX20 elements were applied.

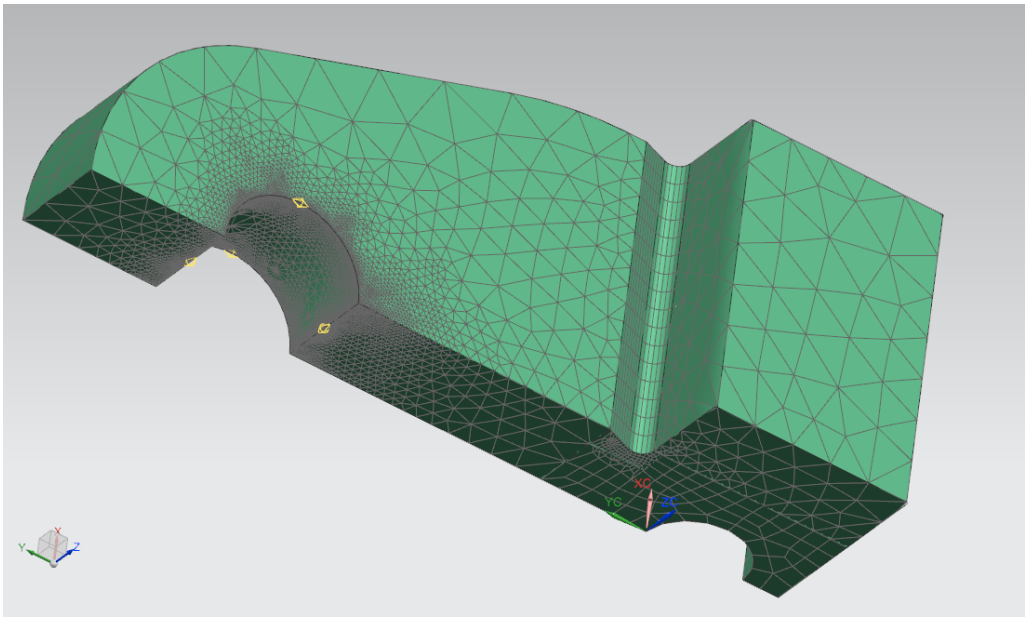

(b) 3D view

Figure 15: FE analysis no.1 - Final mesh

Boundary conditions

Table 9 shows the boundary conditions applied to FE analysis no.1. The force is based on the symmetrical conditions of the FE model: $\frac{2800kN}{4} = 700kN$.

Due to the symmetry of the lifting lug, the symmetric planes is fixed both to translatory and rotatory motion, at the applicable surface on the lifting lug.

Note: DOF is short for Degree Of Freedom and describes how an object can move in a three-dimensional environment.

Boundary conditions

Load			**Fixed constraints/DOF**						
Type	Location	Value	Location	Translation			Rotation		
				X	**Y**	**Z**	**X**	**Y**	**Z**
Force	Main body interface	700kN	YZ - Plane	√			√		
			YX - Plane			√			√
			Shackle hole		√				

Table 9: FE analysis no.1 - Boundary conditions

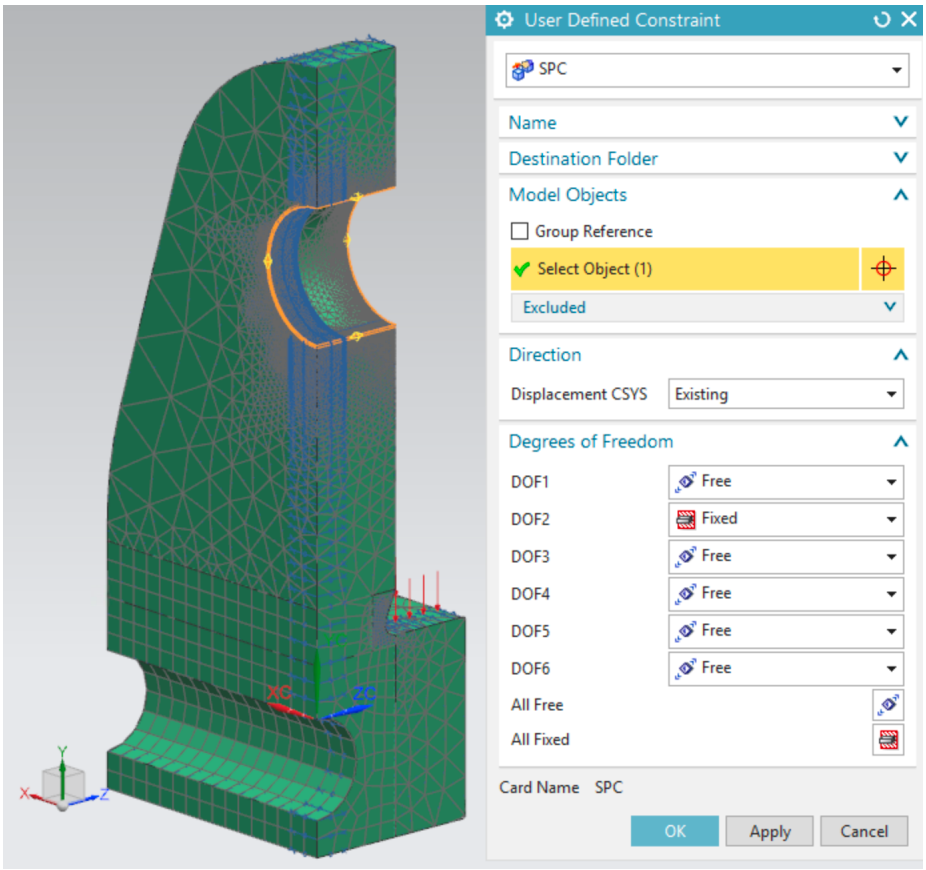

Figure 16: FE analysis no.1 - Boundary conditions at the shackle hole

Results

Table 10 and Figure 17 provides the results of FE analysis no. 1: Lifting lug - Main body.

Results

	Value	Unit	Discussion	Conclusion
Maximum stress	**541**	MPa	Figure 17a shows the stress distribution. The scale is settled to a maximum 550 MPa, which is the acceptance criteria. The highest Von Mises stress is in the curvature at 541 MPa. A singularity at 567 MPa occurs at the shackle hole edge. This is due to the elements fixed position which results in high local stress concentration and could therefore be ignored.	Approved
Maximum displacement	**0.2**	mm	The highest displacement is at the loaded surface and its concluded as a low value compared to its adjacent dimensions. The displacement will not affect the structural integrity of the lifting lug.	Approved

Table 10: FE analysis no.1 - Results. Lifting lug - Main body

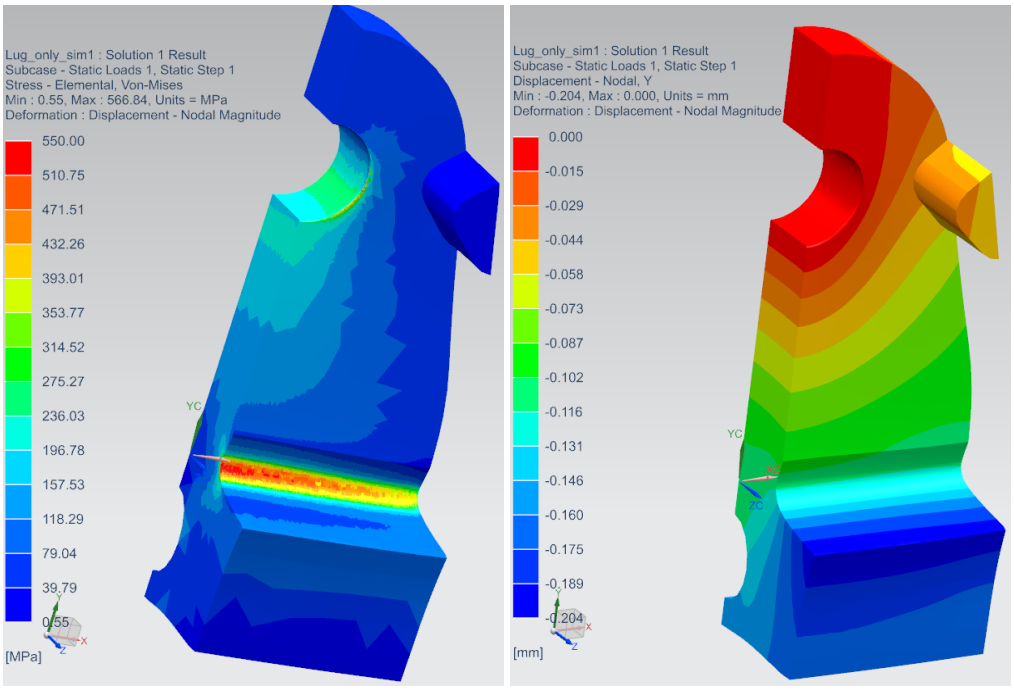

(a) Von Mises stress result

(b) Displacement result

Figure 17: FE analysis no.1 - Results. Lifting lug - Main body

3.2.3 FE analysis no. 2: Main body - Lifting lug. Off-center lift.

This is the first analysis of the main body, analyzing the load transfer between the main body and the lifting lug.

The load transfer could be located in many different positions along the slot in the main body. During the analysis, only two load cases would be analyzed, max off-center lift at 0.5m and center lift. Section 3.1.2 describes the difference. Section 3.2.4 covers center lift

If the body could handle these two positions, it is assumed that it would handle every position in between. It is worth to mention that the end cap, which function as a stiffener, is removed, making the analysis a even more conservative.

Geometry

The geometry of the main body is shown in Figure 18. Notice the coordinate system.

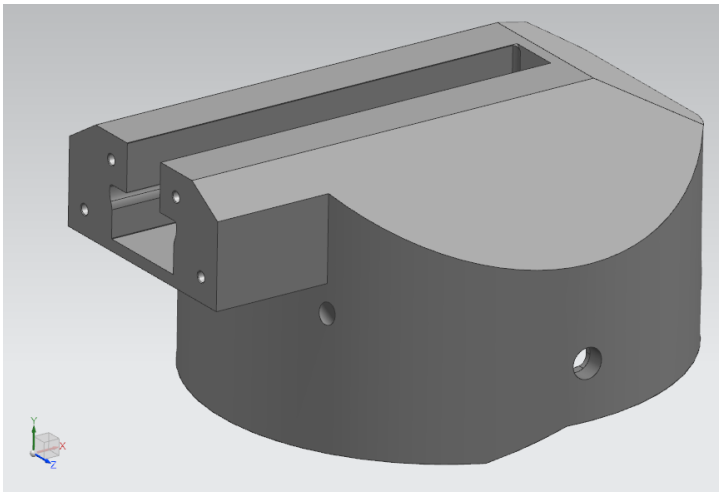

Figure 18: Main body geometry

The main body is symmetric in the XY plane. The lower part of main body is unnecessary material and cut away. This simplification drastically reduce solving time at the cost of accuracy. The symmetric and reduced model shown in Figure 19 represent the FE model. The same model is also used for the next analysis, covered in section 3.2.4.

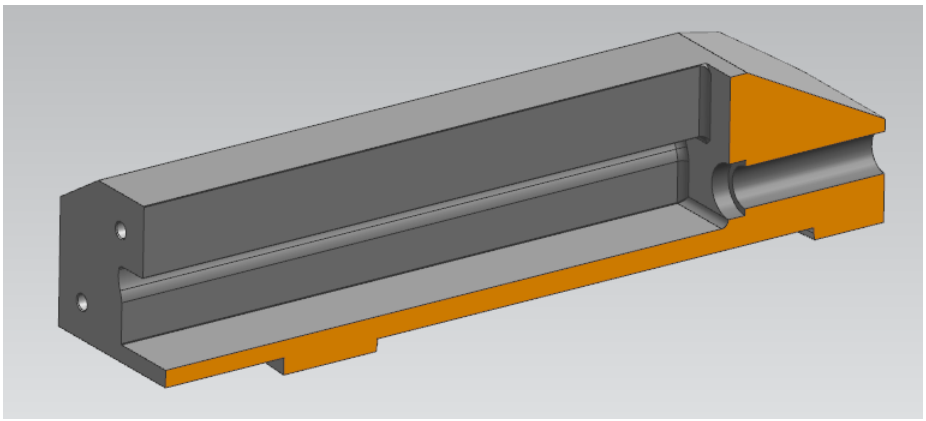

Figure 19: FE model - main body

Mesh

Table 11 and Table 12 covers the mesh strategy and the mesh result, respectively. The following figures shows the meshing process.

Meshing data

Strategy	**Element**		**Features**
The FE model is split into several bodies and meshed with HEX20 and TET10 elements, were HEX20 was applied to the most critical areas. In this case, the critical area is at the curvature, next to the lifting lug support face. Figure 20 shows the curvature.	Type	Size	Split body. Mesh mating command. 3D Swept mesh. 3D Tetrahedral mesh.
	HEX20	2mm	
	TET10	40mm	

Table 11: FE analysis no.2 - Meshing data

Mesh result

Number of elements	Number of nodes
HEX20: 39 000 TET10: 82 910	174 672

Table 12: FE analysis no.2 - Mesh result

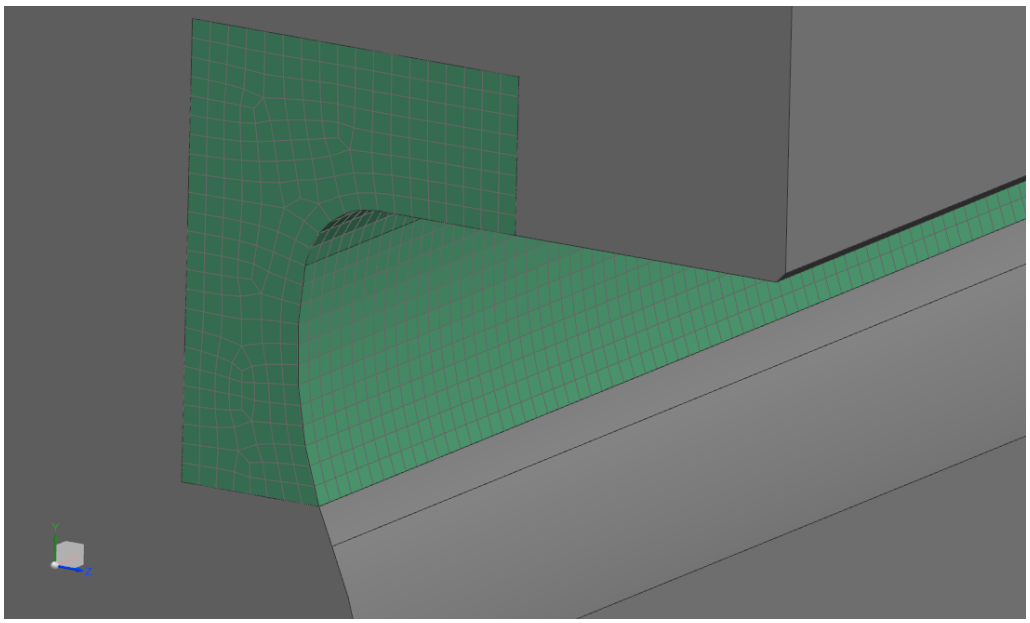

Figure 20: Figure shows the HEX20 elements applied to the curvature

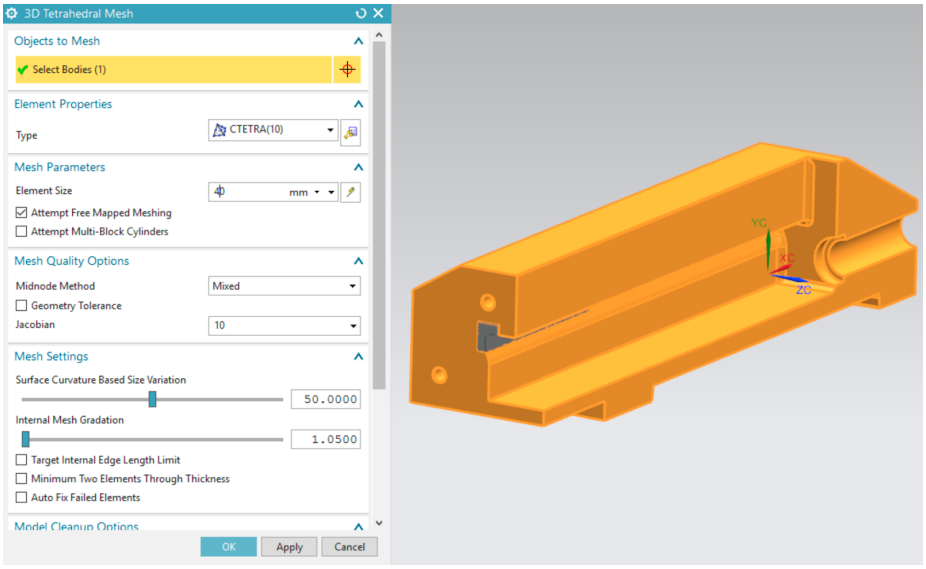

Figure 21: Figure shows TET10 elements being applied to the rest of the body

Boundary conditions

Table 13 shows the boundary conditions applied to FE analysis no.2. The force is based on the symmetrical conditions of the FE model: $\frac{2800kN}{2} = 1400kN$.

Boundary conditions

Load			**Fixed constraints/DOF**							
Type	Location	Value	Location	Translation			Rotation		
				X	**Y**	**Z**	**X**	**Y**	**Z**
Force	Lifting lug interface, off-center position.	1400kN	XZ - Plane	√	√				
			YX - Plane			√			√

Table 13: FE analysis no.2 - Boundary conditions

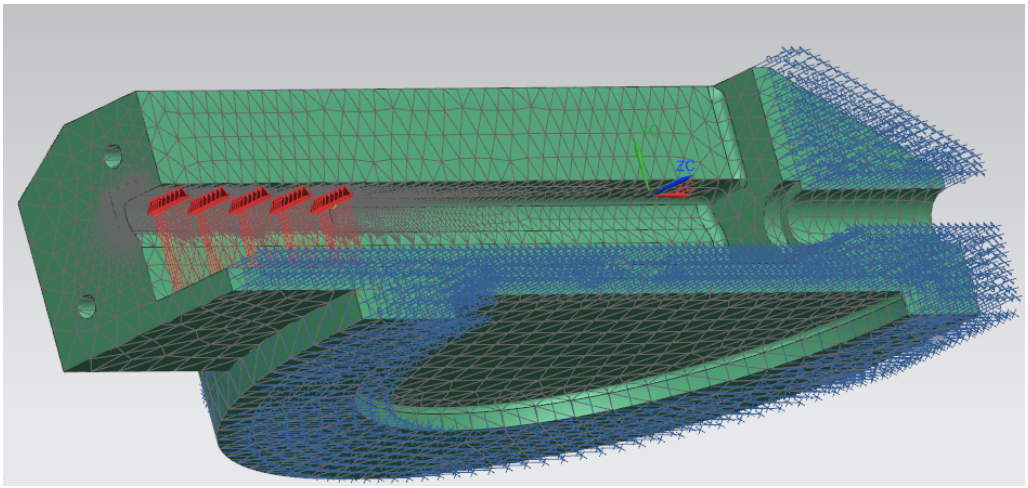

Figure 22: FE analysis no.2 - Boundary conditions at the main body.

Results

Table 14 and Figure 23 and 24 provides the results of FE analysis no. 2: Main body - Lifting lug. Off-center lift.

Results

	Value	Unit	Discussion	Conclusion
Maximum stress	**466**	MPa	Figure 23 shows the stress distribution. The scale is settled to a maximum 550 MPa, which is the acceptance criteria. The highest Von Mises stress is in the curvature at 466 MPa.	Approved
Maximum displacement	**0.53**	mm	This displacement has a relatively low value and will not affect the structural integrity of the main body. Figure 24 shows the displacement distribution in the Y-axis direction. Note the coordinate system.	Approved

Table 14: FE analysis no.2 - Results. Lifting lug - Main body. Off-center lift.

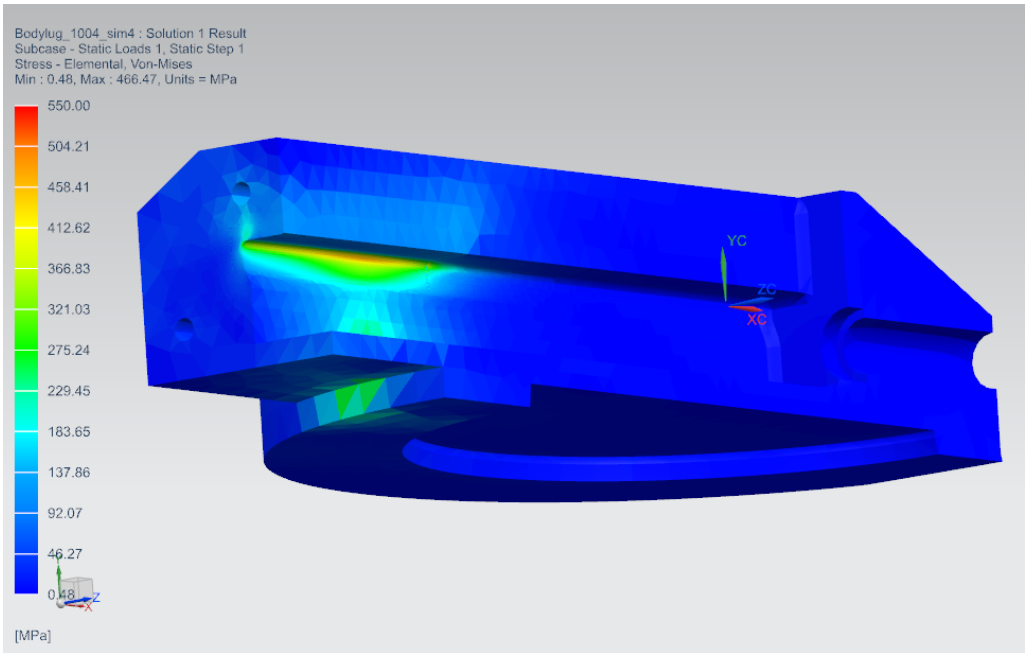

Figure 23: FE analysis no.2 - Results. Maximum stress

3.2.4 FE analysis no. 3: Main body - Lifting lug. Center lift.

This is the second analysis of the main body, analyzing the load transfer between the main body and the lifting lug. This analysis covers center lift, while the previous covered off-center.

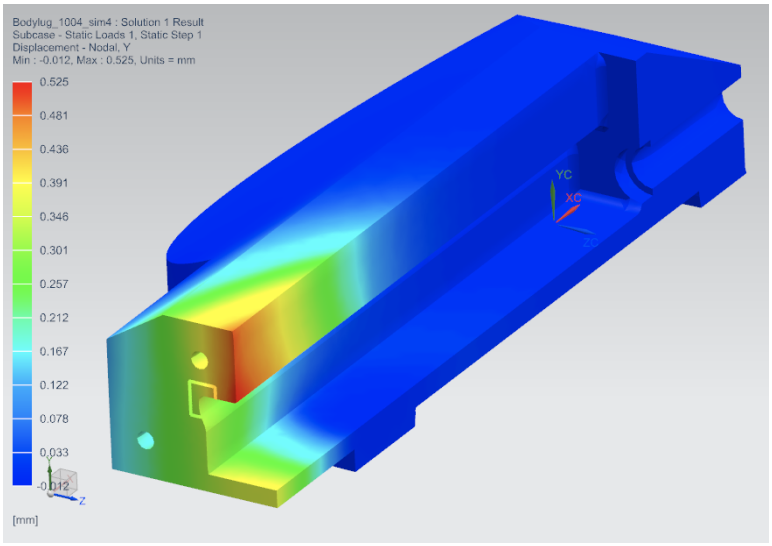

Figure 24: FE analysis no.2 - Results. Maximum displacement.

Geometry

The geometry for this analysis is the same as for the previous analysis, referring to section 3.2.3 - "FE analysis no. 2: Main body - Lifting lug. Off-center lift."

Mesh

Table 15 and Table 16 covers the mesh strategy and the mesh result, respectively. The following Figure 25 shows the finished mesh.

Meshing data

Strategy	**Element**		**Features**
Same mesh strategy as in the previous analysis, referring to section 3.2.3. Only difference is the location of the critical curvature and its HEX20 elements, now located in center.	Type	Size	Split body. Mesh mating command. 3D Swept mesh. 3D Tetrahedral mesh.
	HEX20	2mm	
	TET10	40mm	

Table 15: FE analysis no.3 - Meshing data

Mesh result

Number of elements	Number of nodes
HEX20: 39 000 TET10: 84 555	288 177

Table 16: FE analysis no.3 - Mesh result

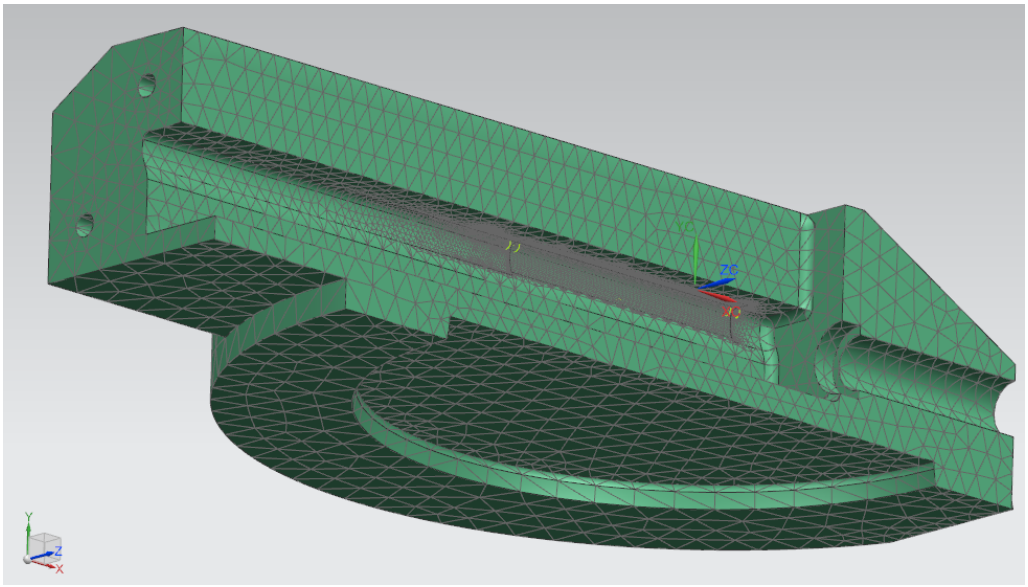

Figure 25: Figure shows the final mesh of the main body.

Boundary conditions

Table 17 shows the boundary conditions applied to FE analysis no.3. Same boundary conditions as for the previous analysis, only difference is the center located force.

Boundary conditions

Load			**Fixed constraints/DOF**						
Type	Location	Value	Location	Translation			Rotation		
				X	**Y**	**Z**	**X**	**Y**	**Z**
Force	Lifting lug interface, center position.	1400kN	XZ - Plane	√	√				
			YX - Plane			√			√

Table 17: FE analysis no.3 - Boundary conditions

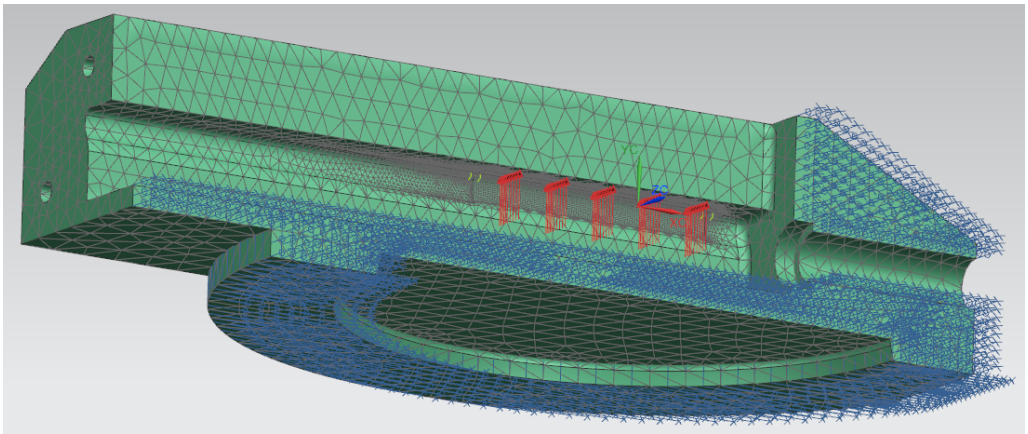

Figure 26: FE analysis no.3 - Boundary conditions at the main body.

Results

Table 14 and Figure 27 and 28 provides the results of FE analysis no. 3: Main body - Lifting lug. Center lift .

Results

	Value	Unit	Discussion	Conclusion
Maximum stress	**290**	MPa	Compared to the previous analysis covered in section 3.2.4, the Von Mises stress is well within the limit and approved.	Approved
Maximum displacement	**0.3**	mm	Compared to the previous analysis covered in section 3.2.4, the displacement is concluded approved.	Approved

Table 18: FE analysis no.3 - Results. Main body - Lifting lug. Center lift.

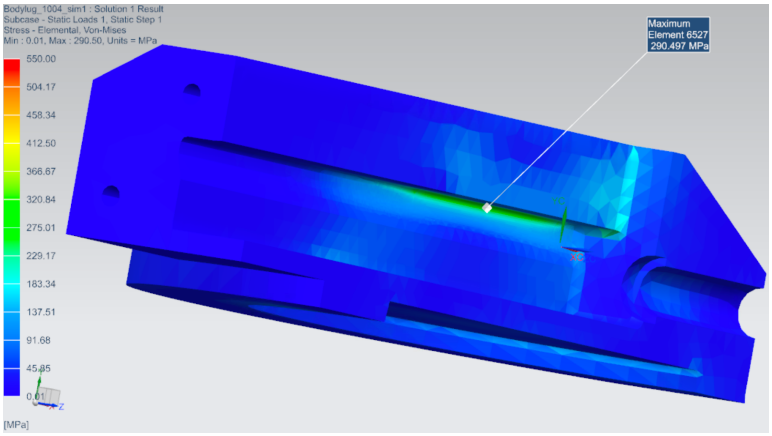

Figure 27: FE analysis no.3 - Results. Maximum stress

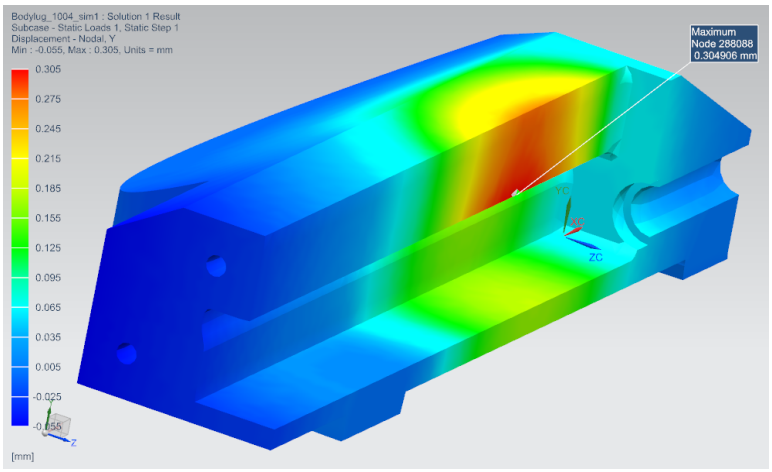

Figure 28: FE analysis no.3 - Results. Maximum displacement in Y-axis direction.

3.2.5 FE analysis no. 4: Main body - Locking dog. Off-center lift.

This analysis covers the main body, analyzing the load transfer between the main body and the locking dogs.

As for the for the two previous analyses, both the off-center and the center load case is relevant, were this analysis covers the off-center case. The worst load case is off-center, as explained in section 3.1.2 -"Load description".

Note: Both the geometry and the mesh are the same for both the off-center and the center analysis.

Geometry

The geometry of the main body is shown in Figure 29. Notice the coordinate system.

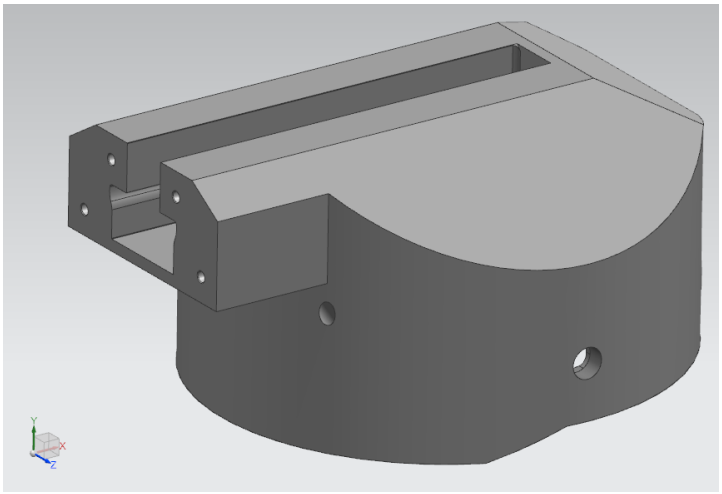

Figure 29: Main body geometry

The main body is symmetric in the XY plane. The upper part of main body is unnecessary material and cut away. This simplification drastically reduce solving time at the cost of accuracy. The symmetric and reduced model is shown in Figure 30b. The same model is also used for the next analysis, covered in section 3.2.5.

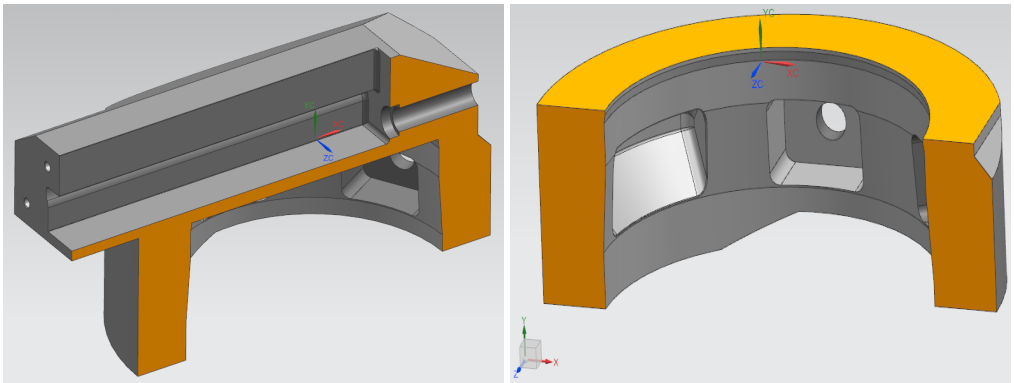

(a) Symmetric FE model (b) Unnecessary material removed. The FE model

Figure 30: Symmetric and reduced model of the the main body.

Mesh

Table 19 and Table 20 covers the mesh strategy and the mesh result, respectively. The following figures shows the meshing process.

Meshing data

Strategy	Element		Features
	Type	Size	Split face.
The housing of the locking dogs in the main body gets loaded at the bottom support face and the two curvatures next to it. As the dogs extends into the H4 profile, the support area will be reduced, as shown in Figure 31b. The support face is therefore split to achieve a more realistic simulation. The mesh density at the edges along the split surface is settled to 1mm. Following the whole FE model is meshed with TET10 elements. Compared to previous analysis and the approach by splitting the body, this approach by splitting the support face is time saving and gives sufficient results. The only disadvantage compared to the previous approach, is that it does not allows square elements.	TET10	30mm	Mesh control. 3D Tetrahedral mesh.

Table 19: FE analysis no.4 - Meshing data

Mesh result	
Number of elements	Number of nodes
TET10: 189 726	331 535

Table 20: FE analysis no.4 - Mesh result

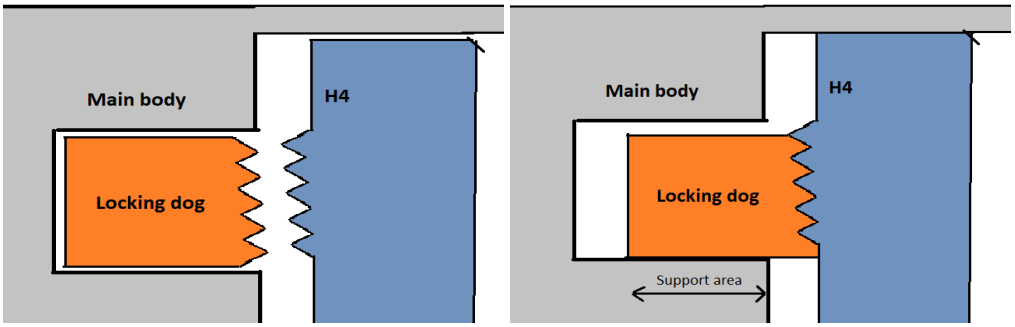

(a) Locking dog retracted (b) Locking dog extended. Note the support face.

Figure 31: Locking dog sequence

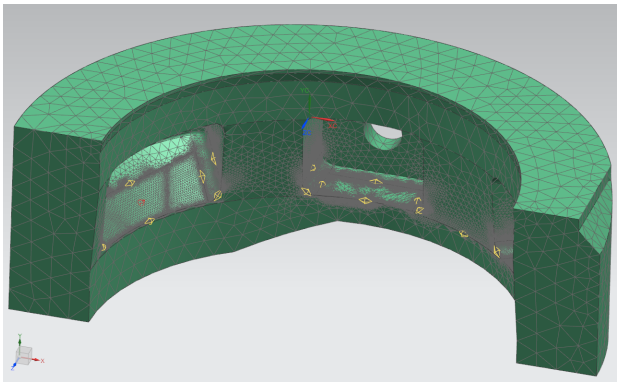

Figure 32: FE analysis no. 4 - Final mesh

Boundary conditions

Before introducing the boundary conditions, some important notes must be mentioned:

- *The load is not distributed evenly across the support surface. The point of attack is located in the locking profile of the dog. This generates a higher force at the edge of the support face and thereby higher pressure in this area. The rear part of dog would probably have its support face in the upper housing. But due to lack of competence of how to have various pressure contribution in a FE analysis, the calculation is simplified and a uniform load is applied to the dogs lower support area.*
- *The housing of the middle dog is not applied with any load. This is an simplification and explained in section 3.1.2.*

Table 21 shows the boundary conditions applied to FE analysis no. 4. Referring to section 3.1.2 - "Load description" and Table 3 for the applied forces. Figure 33 shows a simplified load distribution. Figure 34 shows the boundary conditions applied to the FE model.

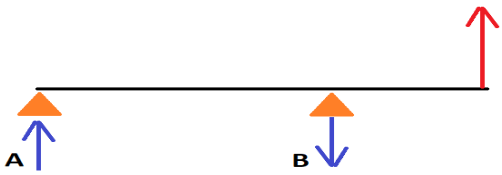

Figure 33: FE analysis no.4 - Simplified load distribution.

Boundary conditions

Load			**Fixed constraints/DOF**							
Type	Location	Value	Location	Translation			Rotation		
				X	**Y**	**Z**	**X**	**Y**	**Z**
Force	A, referring Figure 33	470kN	XZ - Plane	√	√				
			YX - Plane			√			√
Force	B, referring Figure 33	2640kN							

Table 21: FE analysis no.4 - Boundary conditions

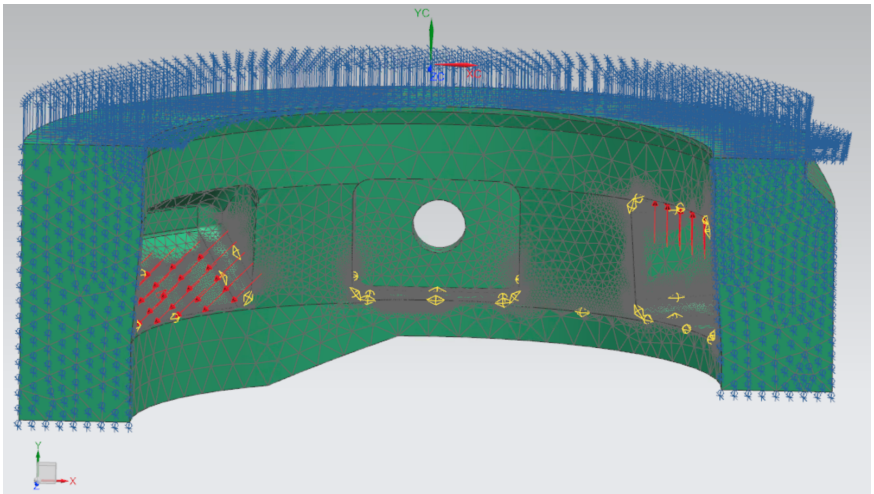

Figure 34: FE analysis no.4 - Boundary conditions at the main body.

Results

Table 22 and the following figures provides the results of FE analysis no. 4: Main body - Locking dog. Off-center lift.

Results

	Value	Unit	Discussion	Conclusion
Maximum stress	**489**	MPa	Figure 35 shows the stress distribution. The highest Von Mises stress is within the requirement and is located at the curvature in the housing of the tilted dog, as Figure 35b shows.	Approved
Maximum displacement	**0.51**	mm	The following itemization covers the displacement in every direction and relates to Figure 36a, 36b and 36c . • Y-direction: 0.23 mm • Z-direction: 0.17 mm • X-direction: 0.51 mm The displacement in Y-direction and Z-direction is considered as low value. The X-direction displacement is on the limit of what is acceptable, as this displacement affect the grip of the locking dogs. However, figure shows that the locking dog support area has a light blue color and displaces with **0.35mm**. This small displacement is considered low enough to not be a risk or increase the risk of failure.	Approved

Table 22: FE analysis no.4 - Results. Main body - Locking dog. Off-center lift.

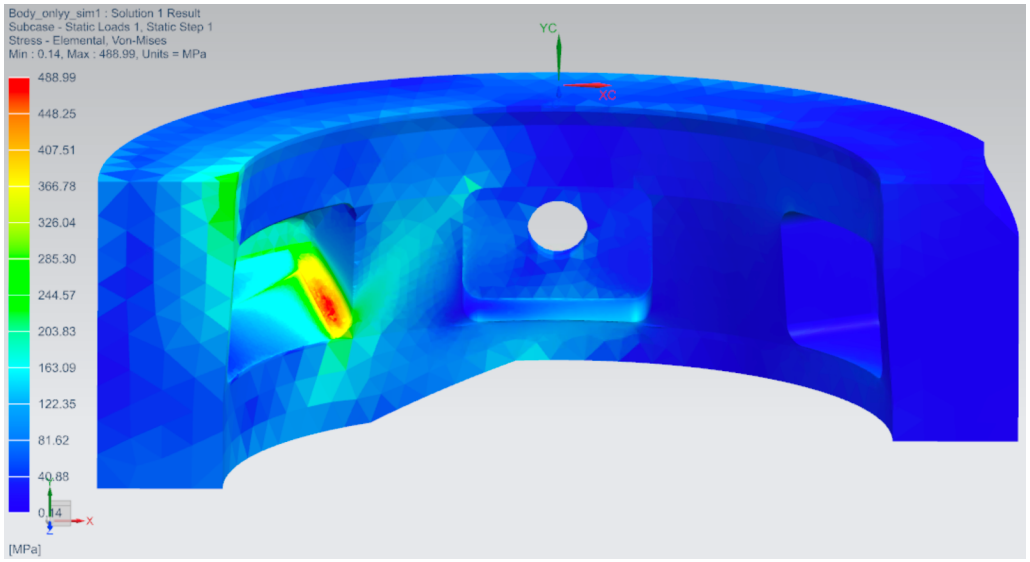

(a) Stress distribution

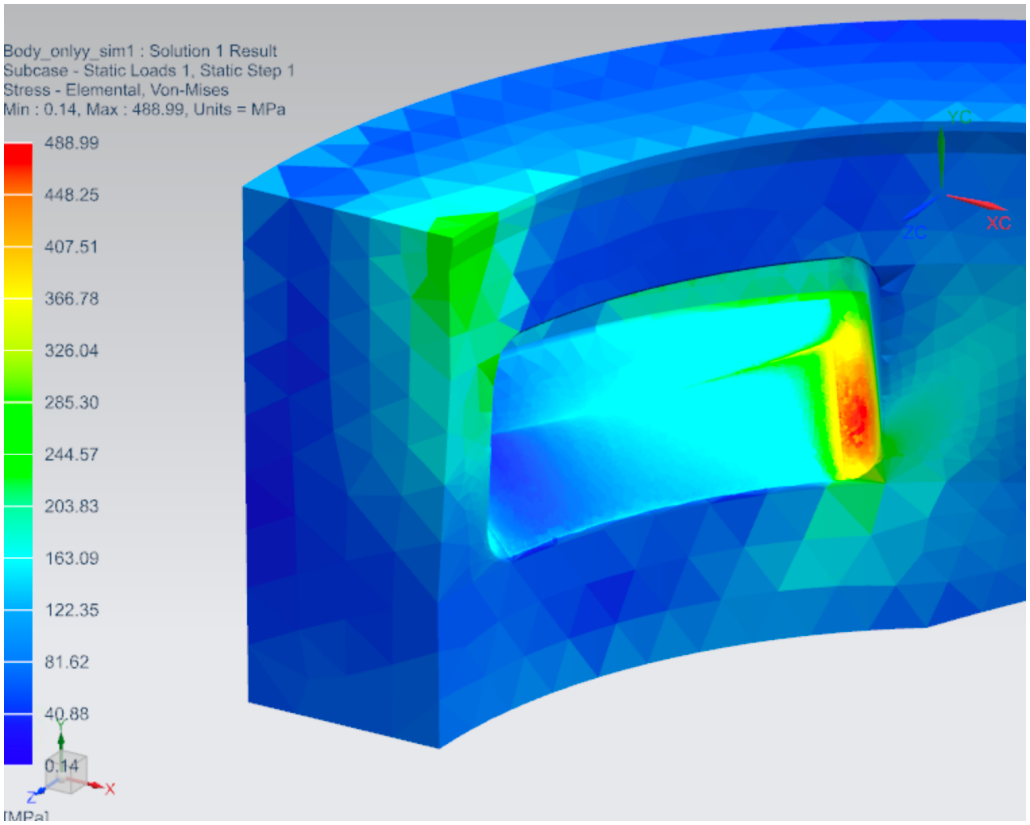

(b) Highest stress concentration area

Figure 35: FE analysis no.4 - Stress results. Main body - Locking dogs. Off-center lift.

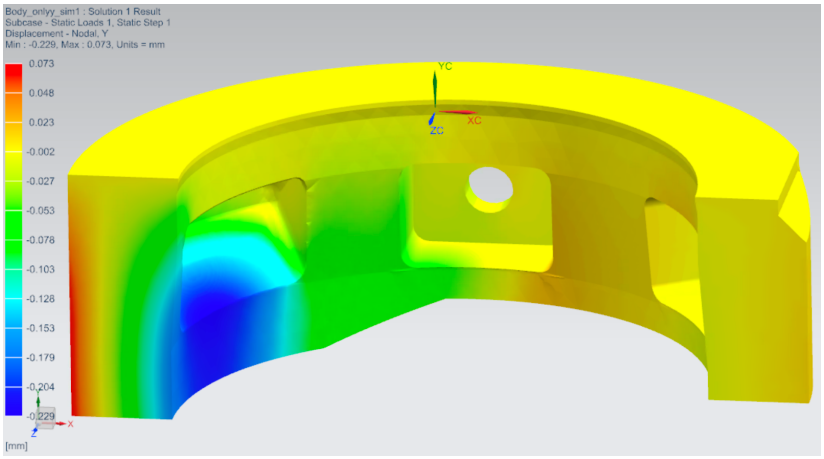

(a) Displacement distribution in Y-direction.

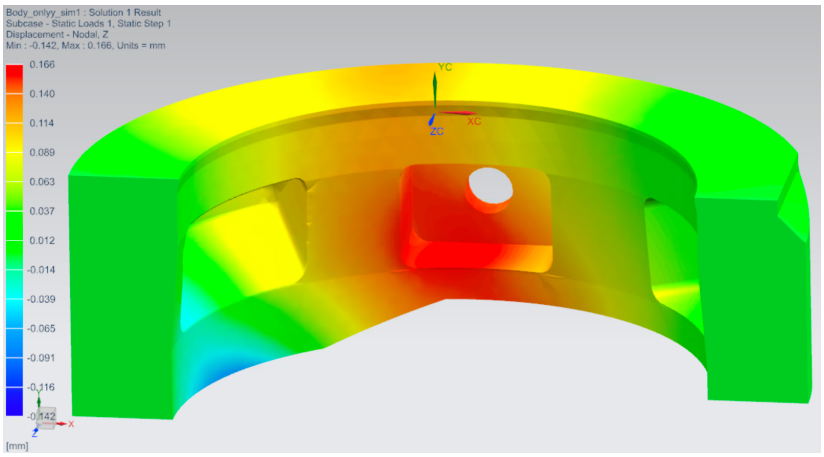

(b) Displacement distribution in Z-direction.

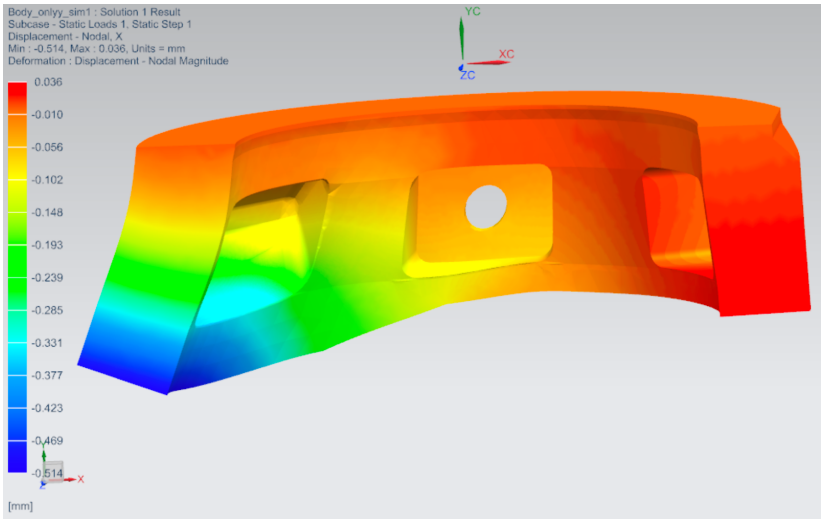

(c) Displacement distribution in X-direction.

Figure 36: FE analysis no.4 - Displacement results.

Note: The displacement illustrated in the figures above is very exaggerated and its so due to the simulation settings.

3.2.6 FE analysis no. 5: Main body - Locking dog. Center lift.

This analysis covers the main body, analyzing the load transfer between the main body and the locking dogs during a center lift. Both the "Geometry" and "Mesh" subsections is similar to the previous analysis and reflect in that analysis, referring to section 3.2.5.

Boundary conditions

Table 23 shows the boundary conditions applied to FE analysis no. 5.

Due to the center positioned lifting point, the load will be evenly distributed to four of the dogs. The two last and tilted dogs, will experience a higher load. The loads and their values is covered in section 3.1.2 - "Load description". Figure 37a and Figure 37b shows the the applied loads.

Note: The first note mentioned in the previous analysis also counts to this analysis, see section 3.2.5 for the note.

Boundary conditions

Load			**Fixed constraints/DOF**						
Type	Location	Value	Location	Translation			Rotation		
				X	**Y**	**Z**	**X**	**Y**	**Z**
Force	Not angled support faces, see Figure 37a.	470kN	XZ - Plane	√	√				
			YX - Plane			√			√
Force	Angled support face, see Figure 37b.	665kN							

Table 23: FE analysis no.5 - Boundary conditions

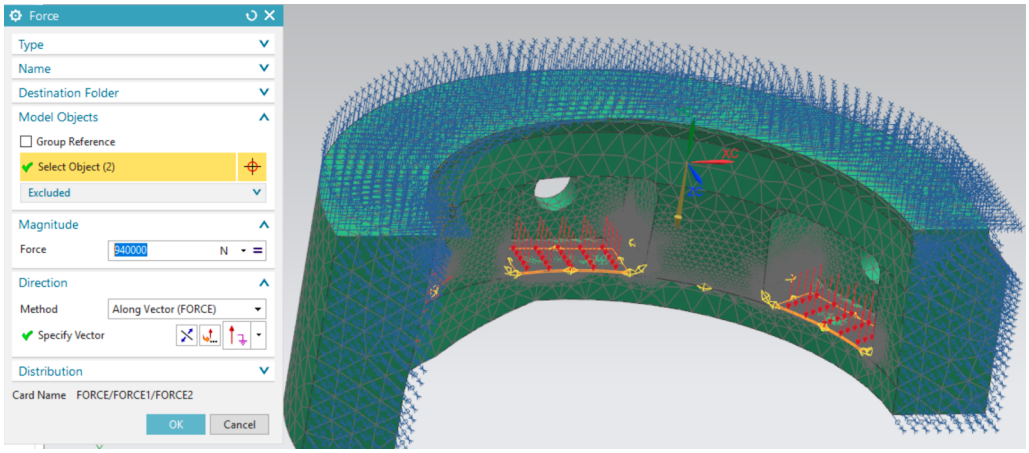

(a) Loads applied to the straight dogs housings.

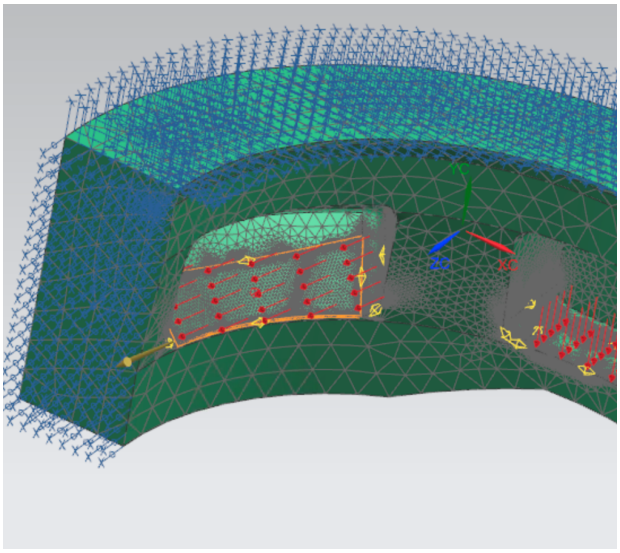

(b) Load applied to the tilted dogs housings.

Figure 37: FE analysis no. 5 - Boundary conditions at the main body.

Results

Table 24 and the FigureThee figures provides the results of FE analysis no. 5: Main body - Locking dog.

Note: The displacement illustrated in the following figures is very exaggerated.

Results

	Value	Unit	Discussion	Conclusion
Maximum stress	**348**	MPa	Figure 38 shows the stress distribution. The highest Von Mises stress is within the requirement and is located at the straight dogs housings.	Approved
Maximum displacement	**0.25**	mm	The following itemization covers the displacement in every direction and relates to Figure 39a, 39b and 39c . • Y-direction: 0.25 mm • Z-direction: 0.09 mm • X-direction: 0.14 mm All the displacement is considered as low value and concluded approved.	Approved

Table 24: FE analysis no.5 - Results. Main body - Locking dog. Center lift.

The the main body withstands both the off-center and center load case, and thereby it will withstand every load case in between.

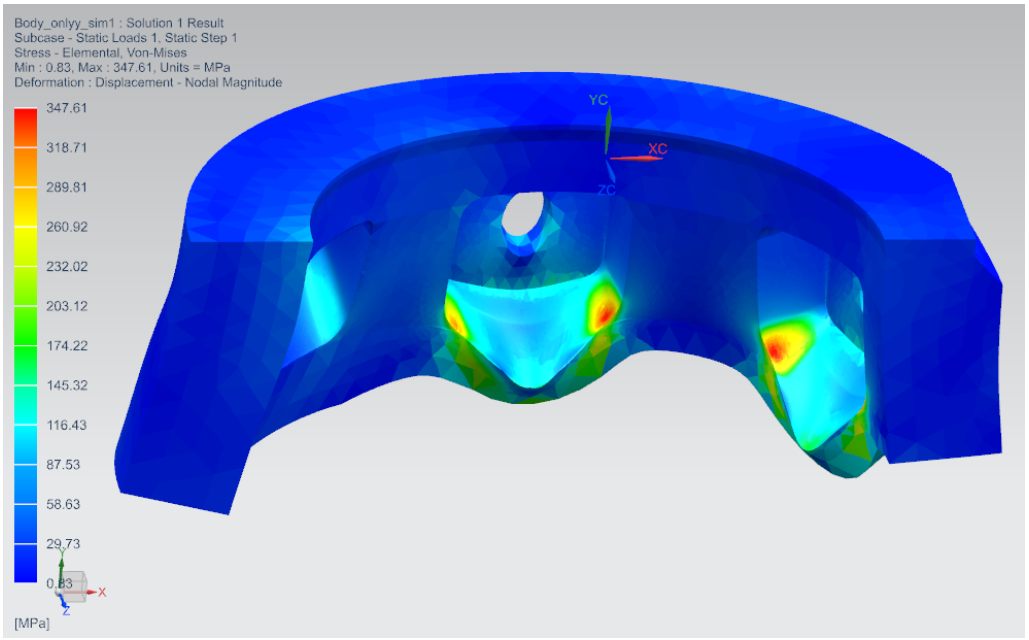

(a) First view

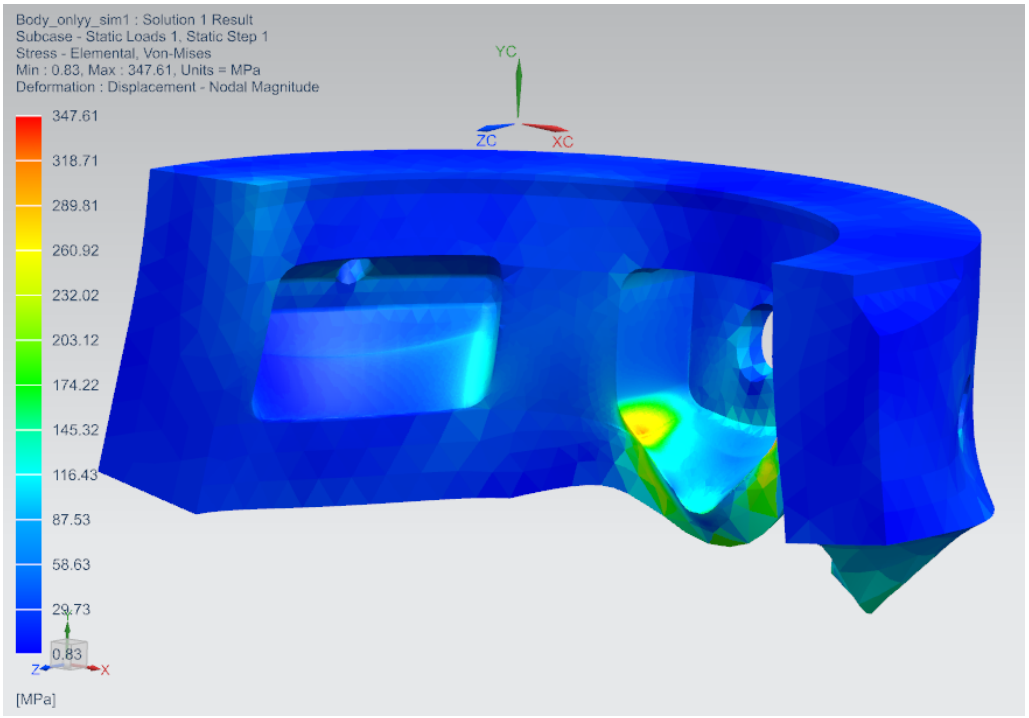

(b) Second view

Figure 38: FE analysis no.5 - Stress results. Main body - Locking dogs. Center lift.

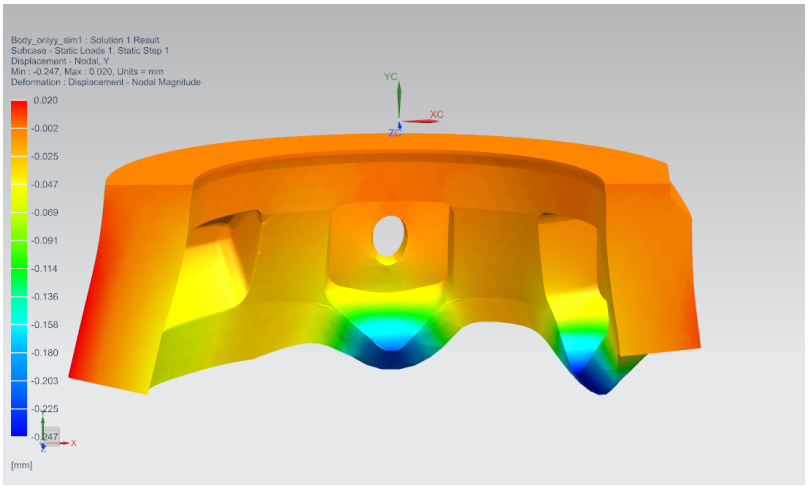

(a) Displacement in Y-direction.

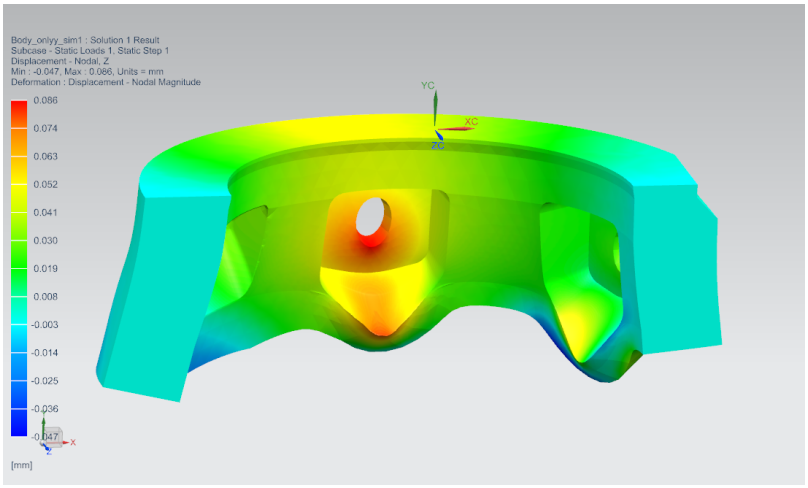

(b) Displacement in Z-direction.

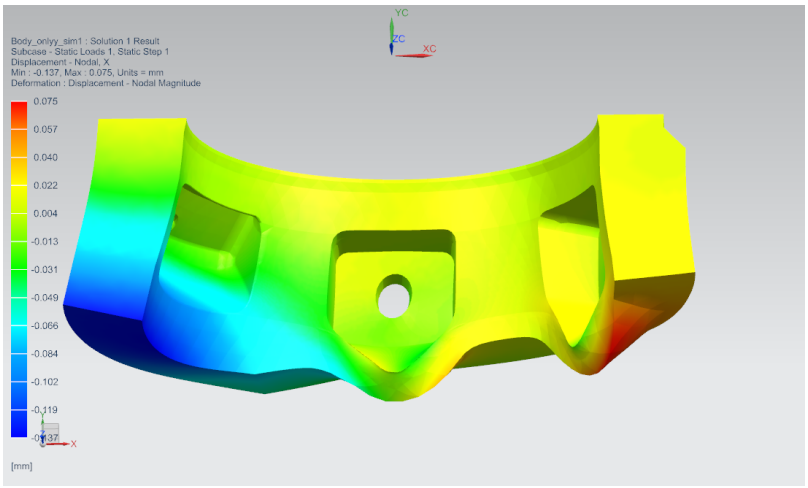

(c) Displacement in X-direction.

Figure 39: FE analysis no. 5 - Displacement results.

3.2.7 FE analysis no. 6: Locking dog - Main body. Straight locking dog.

This analysis covers the straight locking dog, analyzing the load transfer between the main body and the locking dogs.

There are two types of locking dogs in the Xmas Tree Handling Tool (XTHT). The reason for this is explained in the "Main report", while Figure 40 shows the two types.

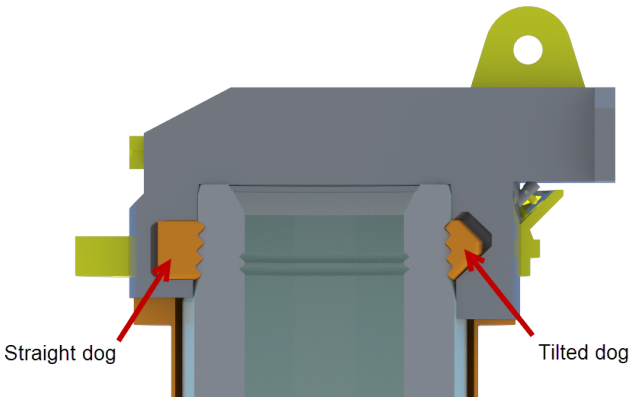

Figure 40: The two type of locking dogs

Geometry

The geometry of the straight locking dog is shown in Figure 41. Figure 41a represent the FE model, while Figure 41b shows the locking dog with the transmission pin assembled. Note the coordinate system.

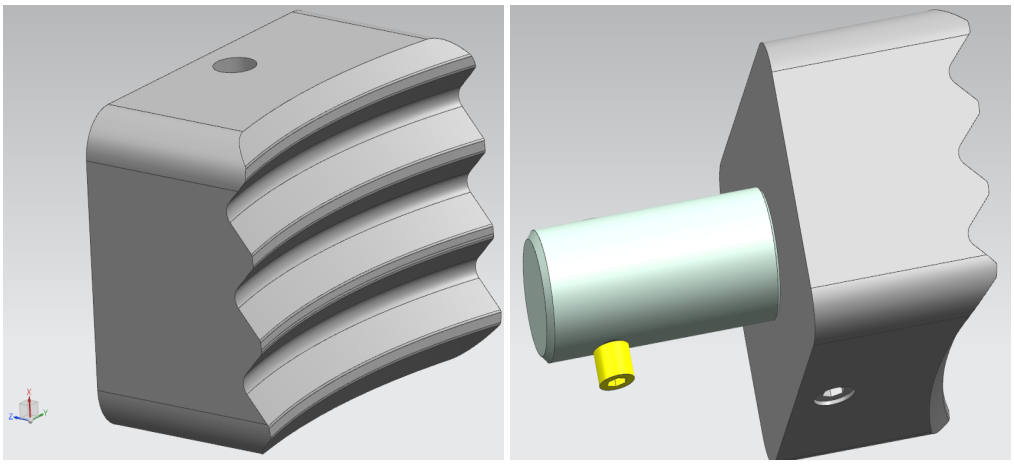

(a) Dog only (b) Locking dog assembly

Figure 41: Straight locking dog geometry

Mesh

Table 25 and Table 26 covers the mesh strategy and the mesh result, respectively. The following Figure 42 shows the finished mesh.

Note: Some errors occurred when trying to create a fine density mesh around the transmission pin hole.

Meshing data

Strategy	**Element**		**Features**
	Type	Size	
The FE model of the straight locking dog is meshed with TET10 elements. Due to the simple geometry, no special approach or features were necessary.	TET10	10mm	3D Tetrahedral mesh.

Table 25: FE analysis no. 6 - Meshing data

Mesh result	
Number of elements	Number of nodes
TET10: 63 384	95 663

Table 26: FE analysis no.6 - Mesh result

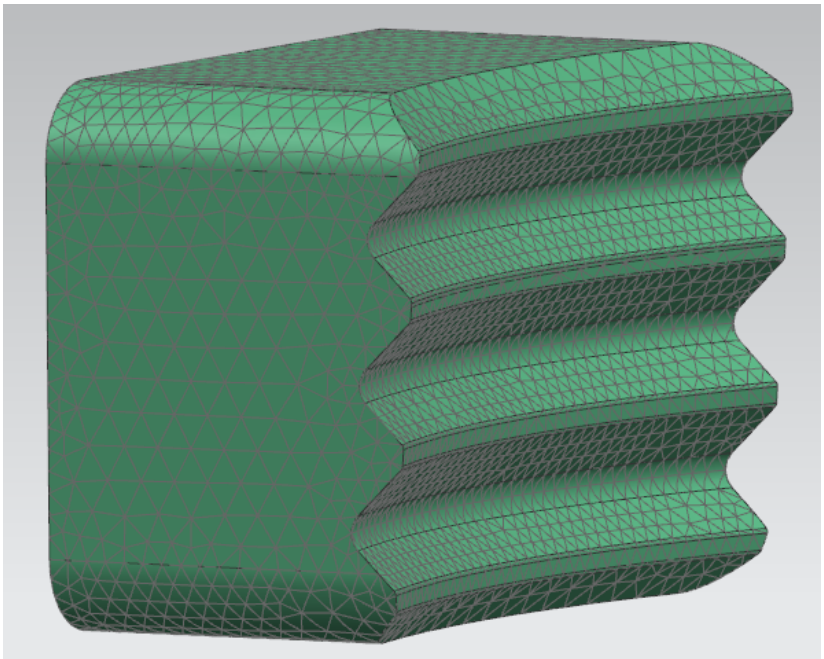

Figure 42: Finished mesh of straight locking dog

Boundary conditions

Table 27 shows the boundary conditions applied to FE analysis no. 6, while Figure 27 shows the FE model and its applied constrains.

During the lift, the straight locking dog would try displace back into its retracted position. The transmission pin prevents this from happening and function as a translation constrain in Z-direction. To simulate this, a additional face in the FE model is made to function as the support area of the transmission pin and thereby constrained in Z-direction.

The loads and their values is covered in section 3.1.2 - "Load description".

Boundary conditions

Load			**Fixed constraints/DOF**						
Type	Location	Value	Location	Translation			Rotation		
				X	**Y**	**Z**	**X**	**Y**	**Z**
Force	Top face of locking profile	665kN	XZ - Plane		√				
			YZ - Plane	√					
			Pin hole			√			

Table 27: FE analysis no. 6 - Boundary conditions

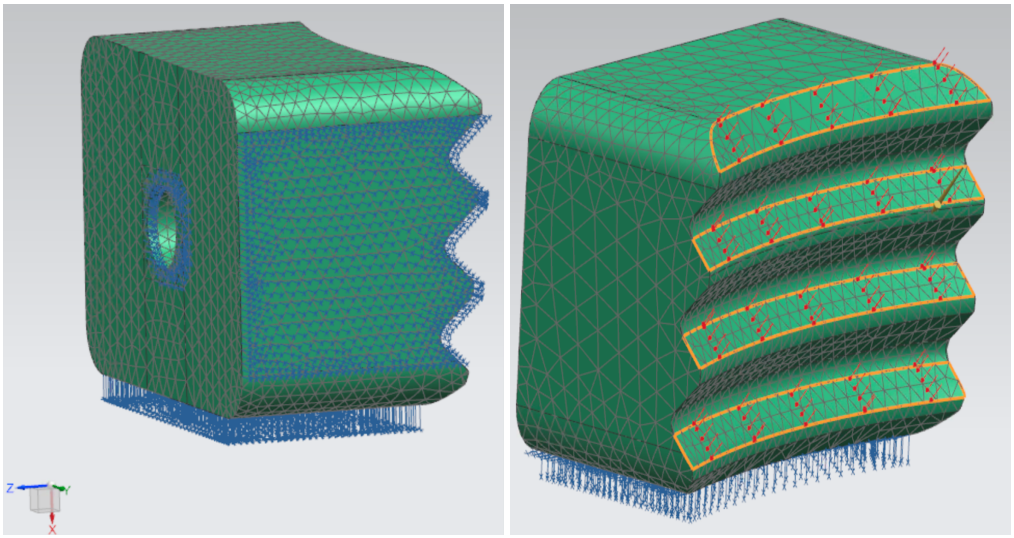

(a) Applied translation constrains. (b) Applied load

Figure 43: FE analysis no. 6 - Boundary conditions at the straight locking dog.

Results

Table 28 and the following figures provides the results of FE analysis no. 6: Straight locking dog - Main body.

Results

	Value	Unit	Discussion	Conclusion
Maximum stress	**197**	MPa	Figure 44 shows the stress distribution. The highest Von Mises stress is located in the contact point between the transmission pin and the locking dog. As mentioned in the "Mesh" section, problems occurred when trying to make a high density mesh in this area. The coarse mesh resulted in a low maximum stress value. The stress would probably converge into higher values along with a finer mesh density, but based on experience its assumed that it will not exceed the maximum stress at 550 Mpa, rather be a lot lower. However, this needs to be controlled.	Need of control
Maximum displacement	**0.03**	mm	The displacement occurs at the edges of the locking dog, as Figure 45 shows. The mesh in this area is sufficient and the result shows that the displacement is low compared to its adjacent dimensions and will not be of any risk. The displacement is measured in X-direction, which was the only relevant direction.	Approved

Table 28: FE analysis no.6 - Results. Straight locking dog - Main body.

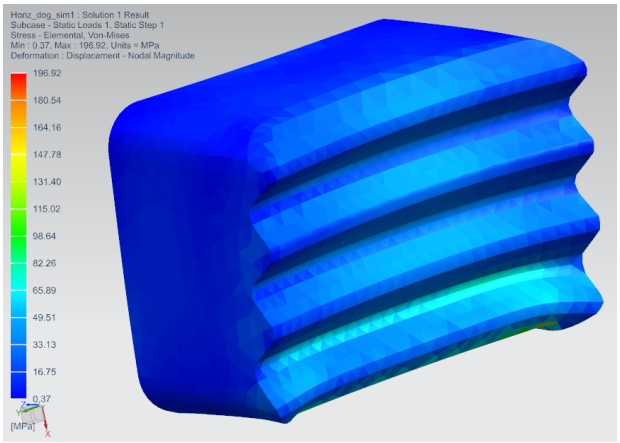

(a) Stress in lock profile

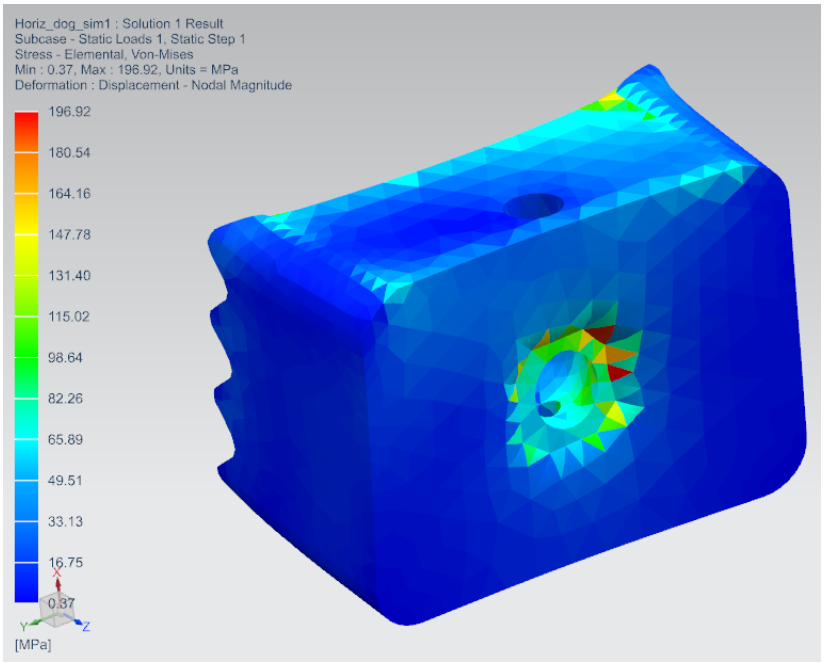

(b) Stress in transmission pin interface

Figure 44: FE analysis no. 6 - Stress result. Straight locking dog - Main body

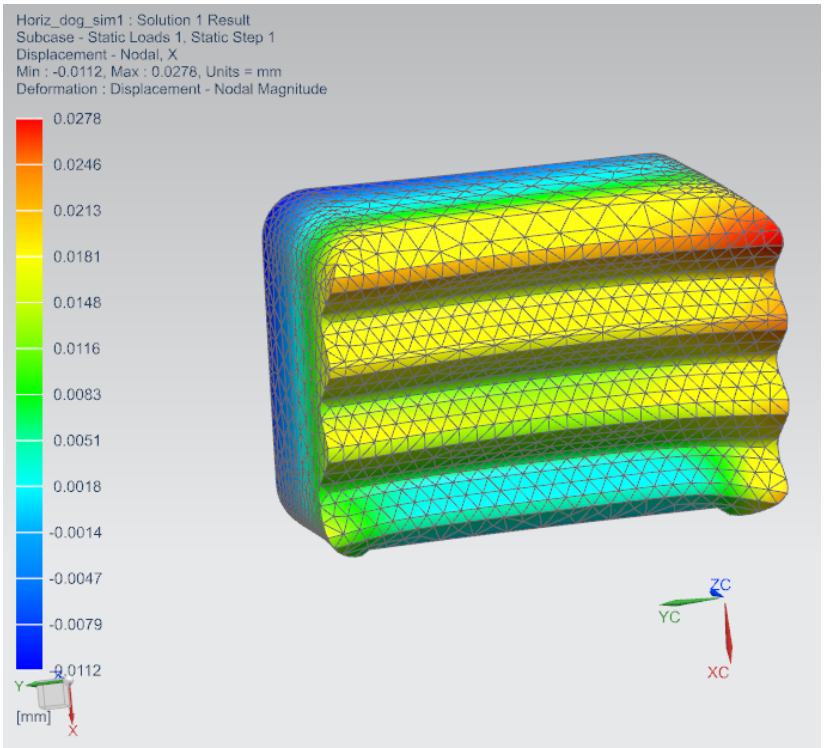

Figure 45: FE analysis no.6 - Displacement result. Straight locking dog - Main body

3.2.8 FE analysis no. 7: Locking dog - Main body. Tilted locking dog.

This analysis covers the tilted locking dog, analyzing the load transfer between the main body and the tilted locking dogs.

Geometry

The geometry of the tilted locking dog is shown in Figure 46. Figure 41a represent the FE model.

The tilted locking dog is symmetric in the XZ plane. Therefore, a symmetric FE model is made to ease the computational process, shown in Figure 46b.

Note: The coordinate system and the dog is not proper aligned to each other. This is due to the tilted dog, but is not a problem as long the boundary conditions is set correctly.

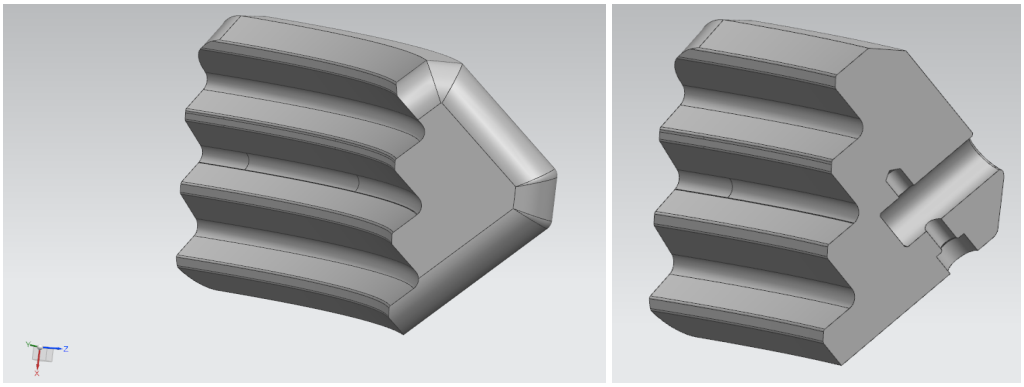

(a) Tilted dog geometry (b) FE model

Figure 46: Tilted locking dog geometry

Mesh

Table 29 and Table 30 covers the mesh strategy and the mesh result, respectively. The following Figure 42 shows the finished mesh.

Meshing data

Strategy	**Element**		**Features**
	Type	Size	
The FE model of the tilted locking dog is meshed with TET10 elements. Due to the simple geometry, no special approach or features were necessary.	TET10	10mm	3D Tetrahedral mesh.

Table 29: FE analysis no. 7 - Meshing data

Mesh result	
Number of elements	Number of nodes
TET10: 14 661	23 873

Table 30: FE analysis no. 7 - Mesh result

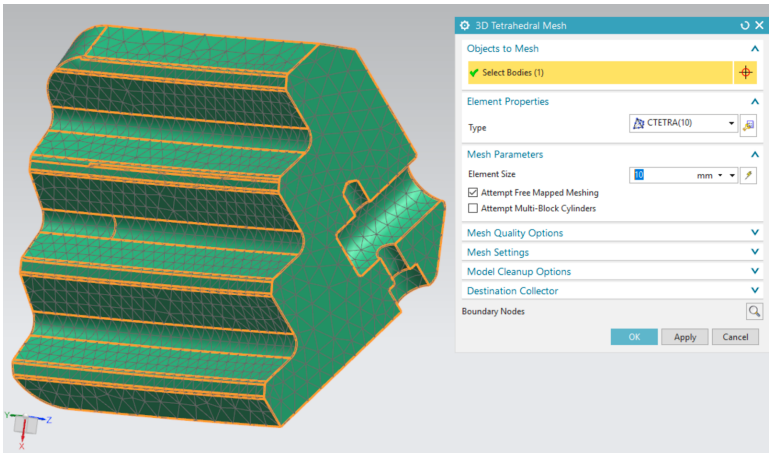

Figure 47: Finished mesh of straight locking dog

Boundary conditions

Table 31 shows the boundary conditions applied to FE analysis no. 7, while Figure 31 shows the FE model and its applied constrains. Symmetric constrains are applied to the XZ-plane at the applicable locking dog surface.

The load and the value is covered in section 3.1.2 - "Load description".

Boundary conditions

Load			**Fixed constraints/DOF**						
Type	Location	Value	Location	Translation			Rotation		
				X	**Y**	**Z**	**X**	**Y**	**Z**
Force	Top face of locking profile	1320kN	XZ - Plane		√			√	
			YZ - Plane / Main body support area	√		√			

Table 31: FE analysis no. 7 - Boundary conditions

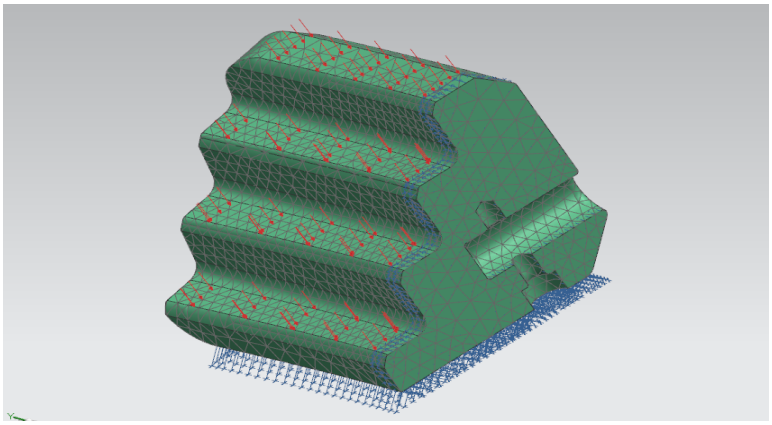

Figure 48: FE analysis no. 7 - Boundary conditions at the tilted locking dog.

Results

Table 32 and the following figures provides the results of FE analysis no. 7: Tilted locking dog - Main body.

Note: The displacement is very exaggerated.

Results

	Value	Unit	Discussion	Conclusion
Maximum stress	**371**	MPa	Figure 49 shows the stress distribution. The highest Von Mises stress is located in at the edge of the bottom constrain, as Figure 49b. This stress concentration occurs due to the great stress difference between the fixed and unfixed elements. This would not occur in reality as the transition between the support are and the back of the lug is smooth with a large radius. However, the allover stress distribution is well within the requirement.	Approved
Maximum displacement	**0.13**	mm	The displacement occurs at the edges of the locking dog, as Figure 45 shows. The itemization shows the highest displacement in every direction. • Z direction: 0.13 mm • Y direction: 0.09 mm • X direction: 0.08 mm The displacement is close to zero in every direction and considered as low value compared to its adjacent dimensions.	Approved

Table 32: FE analysis no. 7 - Results. Tilted locking dog - Main body.

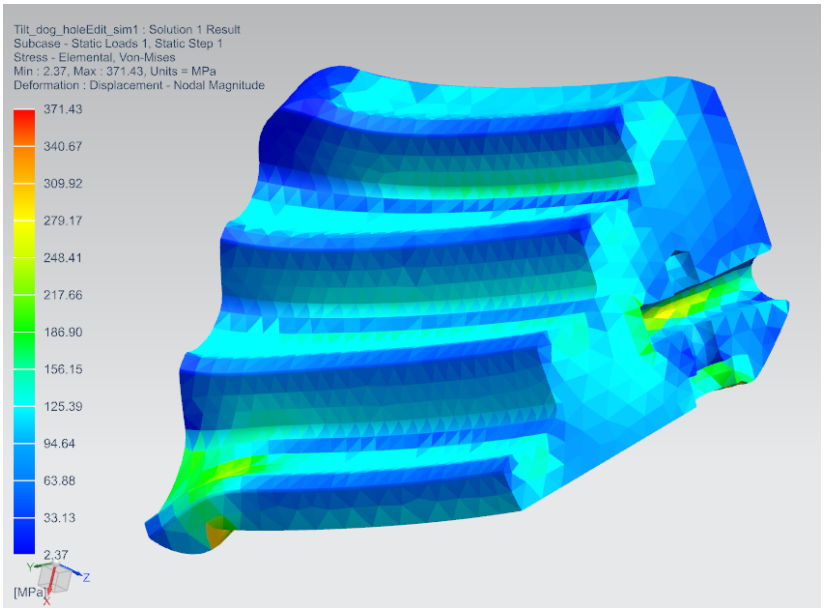

(a) Stress in lock profile

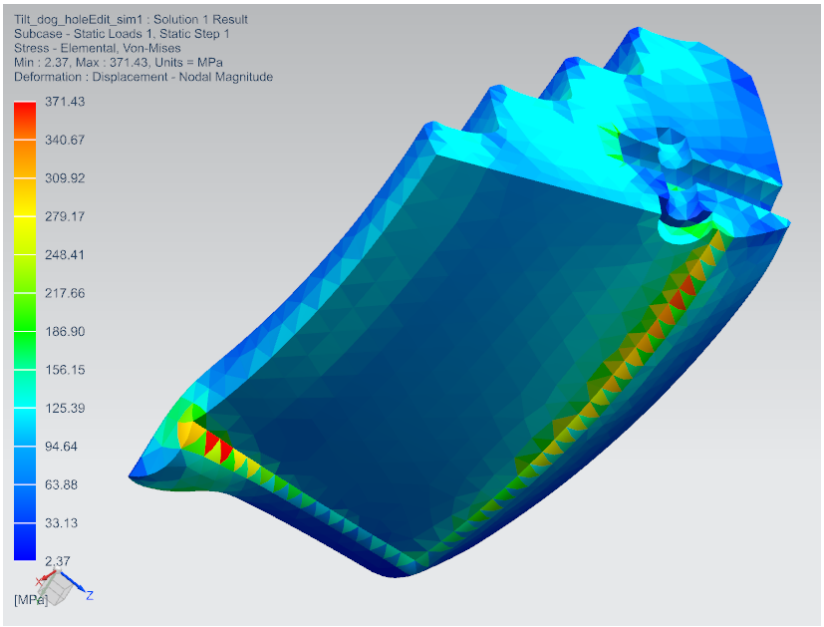

(b) Stress in the locking dog support face. As the displacements shows, the edges would try to wrap itself around the constrained surface, in reality the edges would also be supported.

Figure 49: FE analysis no. 7 - Stress result. Tilted locking dog - Main body

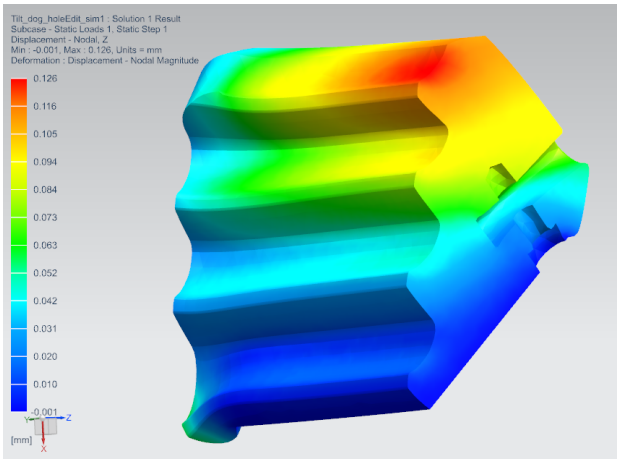

(a) Displacement distribution in Z-direction.

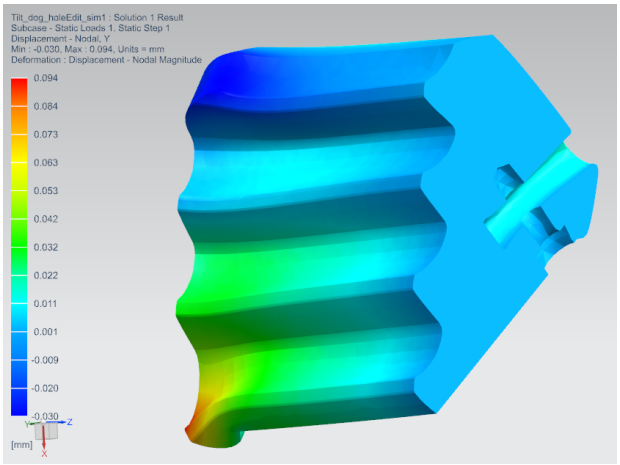

(b) Displacement distribution in Y-direction.

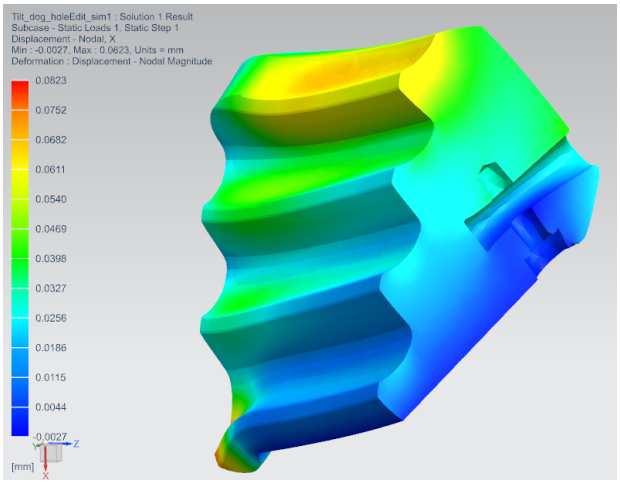

(c) Displacement distribution in X-direction.

Figure 50: FE analysis no. 7 - Displacement result. Tilted locking dog - Main body

3.2.9 FE analysis no. 8: Locking ring - Transmission pins.

This analysis covers the locking ring, analyzing the load transfer between the straight locking dogs and the locking ring.

Geometry

The geometry of the locking ring is shown in Figure 46, which also represent the FE model.

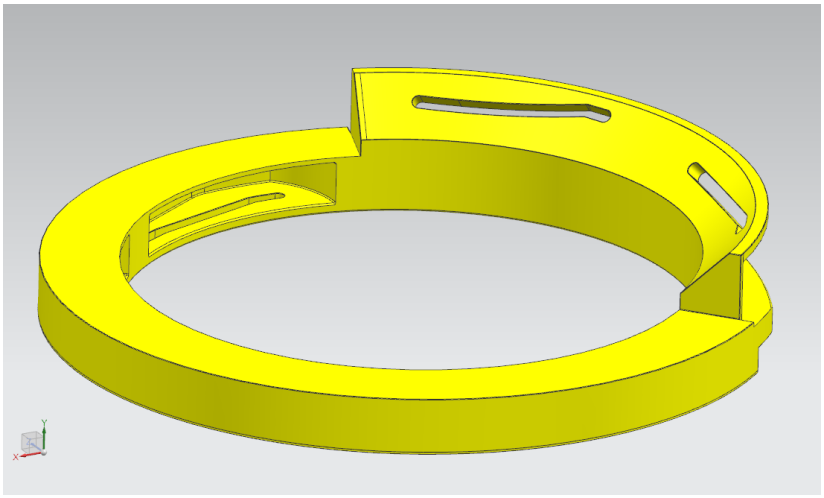

Figure 51: Locking ring geometry

Mesh

Table 33 and Table 34 covers the mesh strategy and the mesh result, respectively. The following Figure 42 shows the finished mesh.

Meshing data

Strategy	**Element**		**Features**
	Type	Size	Split face.
Many surfaces at the locking ring is divided into separate faces, which is going to have their own mesh density. This is necessary due to the boundary conditions applied, covered in the next subsection. The mesh density along with the split surface is settled to 1mm, as shown in Figure 52b. The rest of the locking wheel is meshed with TET10 elements.	TET10	25mm	Mesh control. 3D Tetrahedral mesh.

Table 33: FE analysis no. 8 - Meshing data

Mesh result

Number of elements	Number of nodes
TET10: 285 152	492 1855

Table 34: FE analysis no. 8 - Mesh result

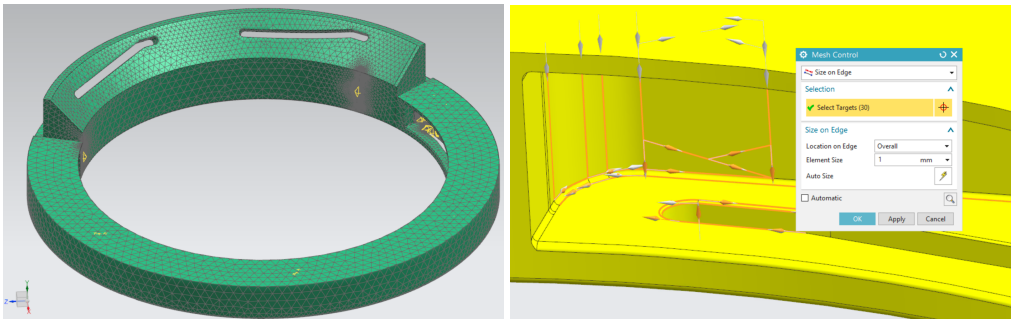

(a) Finished mesh. Note the higher density areas and their yellow dots

(b) High density mesh applied to split surface edges

Figure 52: Finished mesh of locking ring

Boundary conditions

Table 35 shows the boundary conditions applied to FE analysis no. 8, while Figure 35 shows the FE model and its applied boundary conditions.

During lifting, only four of the total six locking dogs would experience force which is pushes it out of its locking profile (referring to section 3.1.2 - "Load description"). The transmission pin transmits the load into the locking wheel. To achieve equilibrium, the locking ring needs to have a support face, resting on the main body. This load scenario is shown in Figure 53.

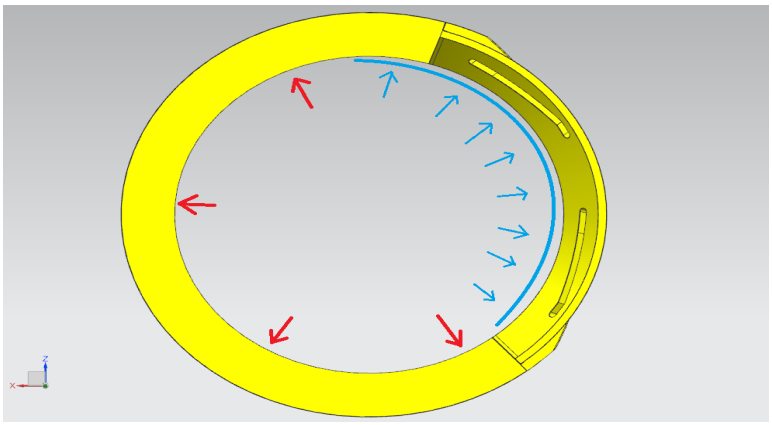

Figure 53: Locking ring load scenario. Red arrows symbolize the locking dogs pushing outwards. The blue arrows symbolize the ring resting on the body

Notes:

- *This analysis reflects a center lift, as this is worst lifting scenario for the locking ring.*
- *Regarding the connection between the locking ring support face and the main body, a tolerance study is necessary. This is mentioned as further work in the main report of the bachelor thesis.*
- *The XZ-plane is constrained at the whole surface underneath the locking ring. In reality its only partially support. However, this constrain is considered sufficent as there are no forces acting in this direction.*

Boundary conditions

Load			Fixed constraints/DOF						
Type	Location	Value	Location	Translation			Rotation		
				X	Y	Z	X	Y	Z
Force (Single)	Support area of transmission pin.	465kN	Main body support face.	√		√			
			XZ - plane		√				

Table 35: FE analysis no. 8 - Boundary conditions

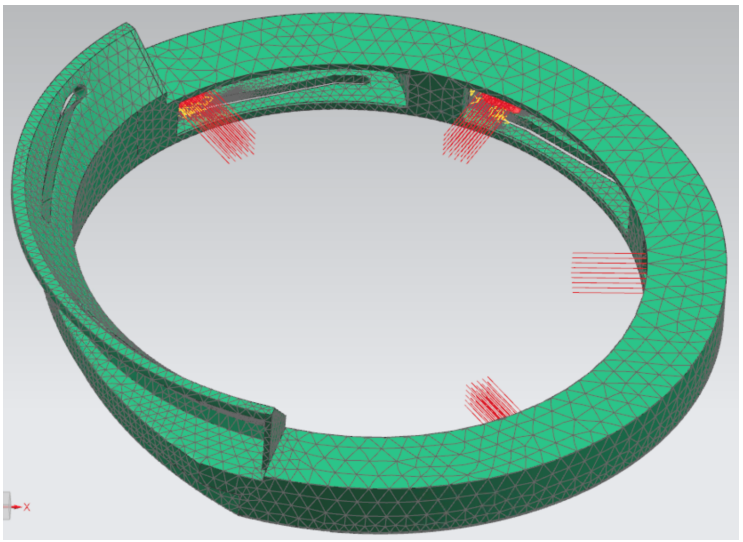

(a) Load applied to transmission pins support faces

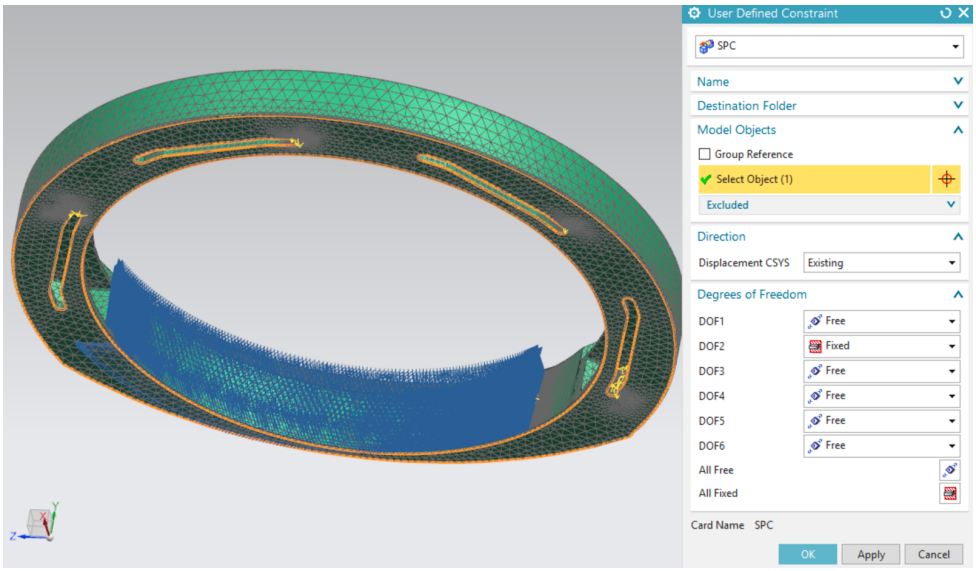

(b) Constrains applied. In reality the ring would rest on four brackets, which means that this constraint is not optimal. But it will give a good estimate

Figure 54: FE analysis no. 8 - Boundary conditions at the locking ring.

Results

Table 36 and the following figures provides the results of FE analysis no. 8: Locking ring - Transmission pin.

Note: The displacement is very exaggerated.

Results

	Value	Unit	Discussion	Conclusion
Maximum stress	**680**	MPa	Figure 55 shows the stress distribution. The highest Von Mises stress is located at a small area in the guiding slot, as Figure 55c. Based on conversations with Aker Solutions, such high stress concentrations at small and local areas can be approved, see meeting report nr.15 in appendix J. Otherwise, the stress generated through the locking ring is well within the requirement.	Approved
Maximum displacement	**0.93**	mm	Figure 56 and figure shows the stress contribution in X-direction and Z-direction, which is the only relevant directions in this analysis. The itemization shows the highest displacements. • Z direction: 0.93 mm • X direction: 0.90 mm The displacement in Z-direction is highest at 0.66mm and lowest at 0.27mm (opposite side), making a total displacement at $0.66mm + 0.27mm = 0.93mm$. The displacements in these direction is crucial and important as it affect the locking dogs engagement to the H4 profile. Considering these values with all its conservative factors mentioned in section 3.1.5, a highest displacement at 0.9mm is considered as sufficient and would not be of any risk or increase the risk of failure.	Approved

Table 36: FE analysis no. 8 - Results. Locking ring - Transmission pin.

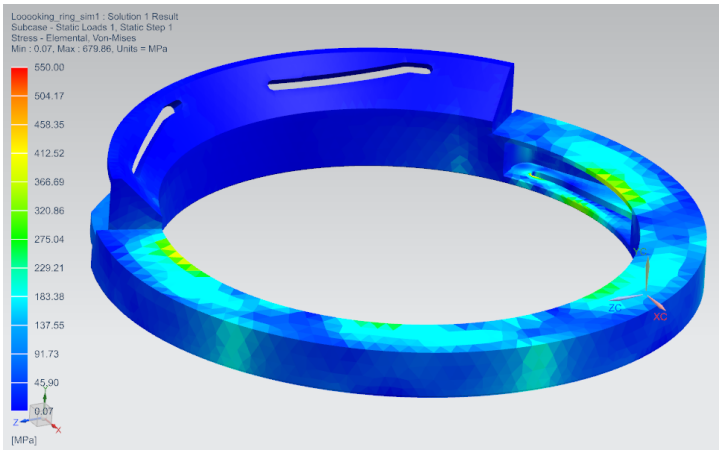

(a) First view

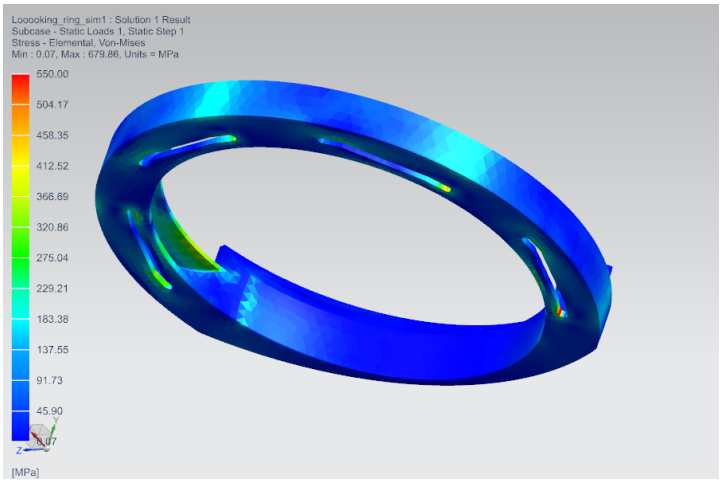

(b) Second view

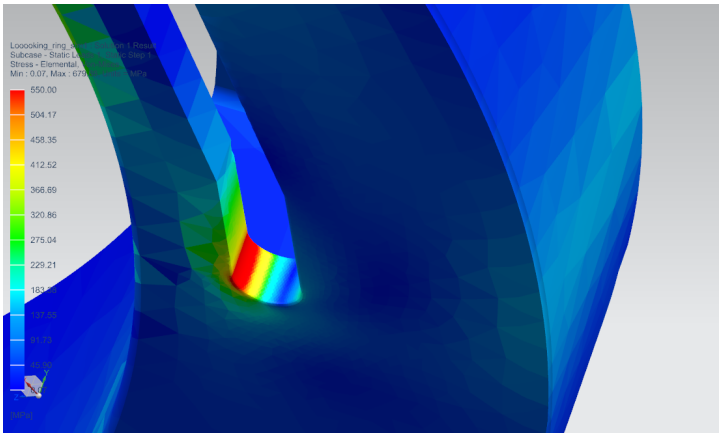

(c) Detail view of local and high stress area.

Figure 55: FE analysis no. 8 - Stress result. Locking ring - Transmission pin.

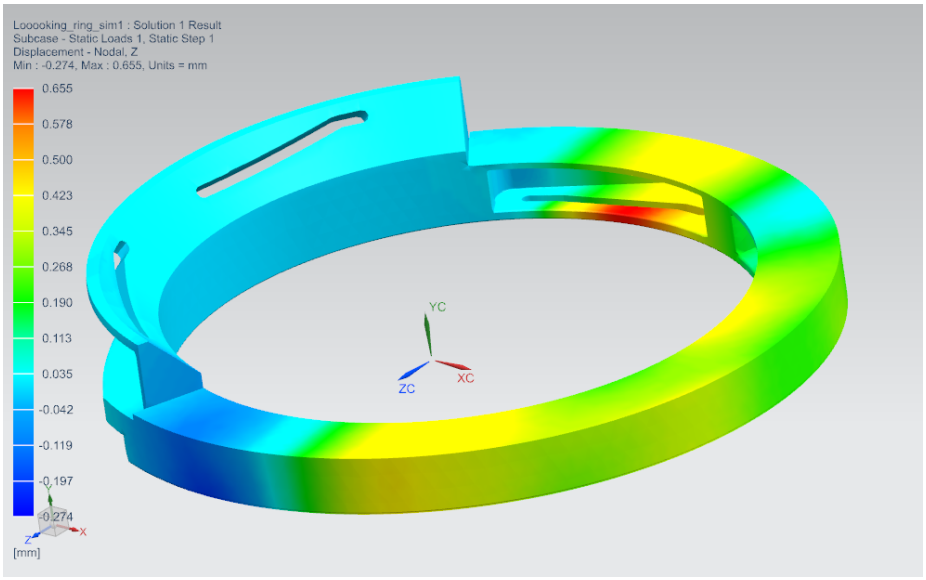

(a) Displacement distribution in Z-direction.

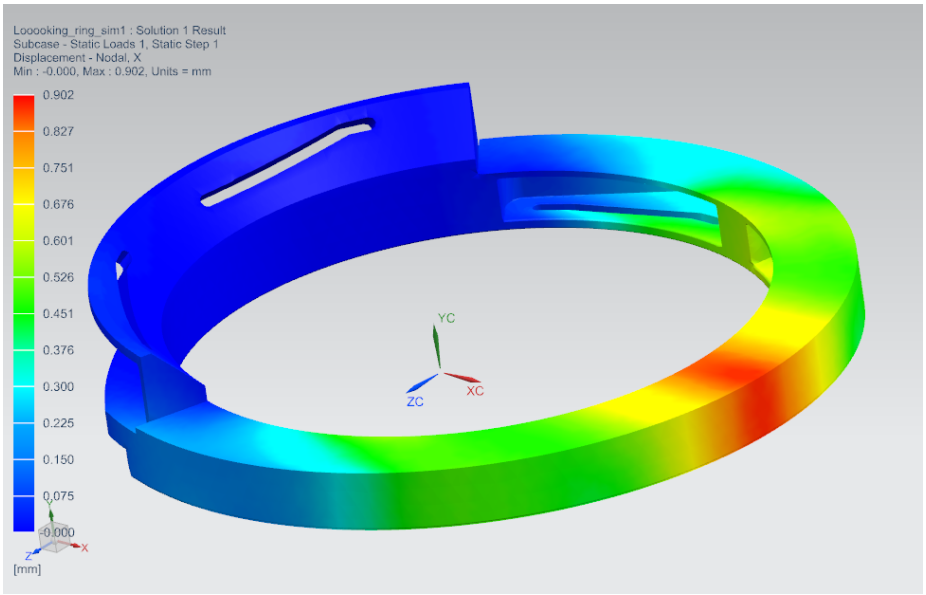

(b) Displacement distribution in X-direction.

Figure 56: FE analysis no. 8 - Displacement result. Locking ring - Transmission pin

3.2.10 FE analysis no. 9: Funnel - Anti-rotation pin

This analysis covers the funnel, analyzing the load transfer between the anti-rotation pin and the locking ring.

The rotation issue and the need of an anti-rotation solution is covered in Appendix E - Angle offset and torque calculations

Geometry

The geometry of the funnel is shown in Figure 57. Figure 57b represent the FE model.

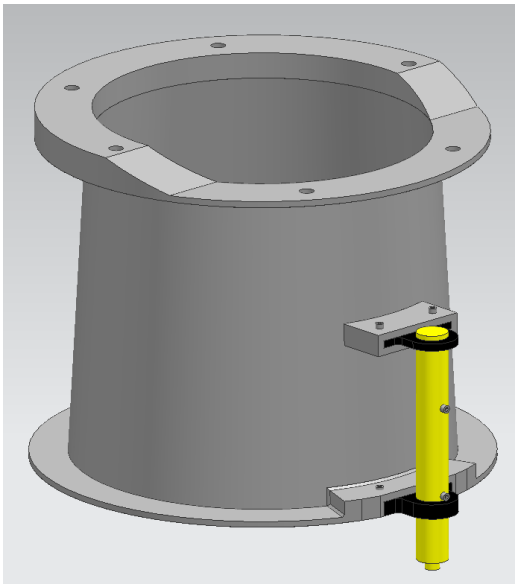

(a) Funnel assembled with the anti-rotation pin.

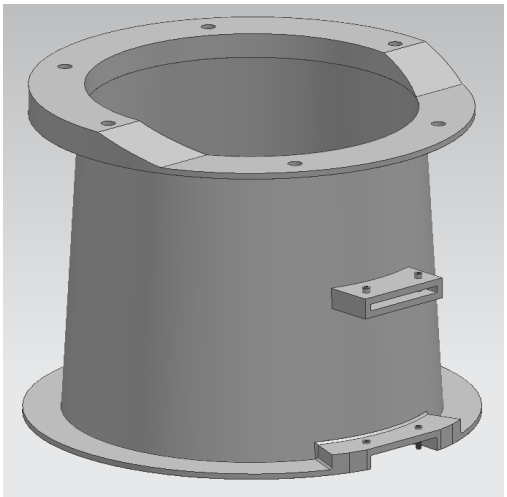

(b) FE model

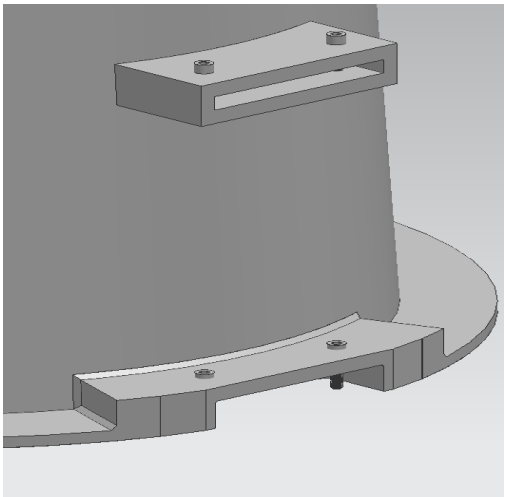

(c) The bracket housings

Figure 57: Funnel geometry

Note: The anti-rotation pin is assembled with two brackets, which is assembled to the funnel by position them in the bracket housings and lock them with bolts.

Mesh

Table 37 and Table 38 covers the mesh strategy and the mesh result, respectively. The following Figure 58 shows the finished mesh.

Meshing data

Strategy	**Element**		**Features**
	Type	Size	Mesh control.
The FE model of the funnel is meshed with TET10 elements. The areas were the loads are applied would experience high stress and therefore these are solved with a higher mesh density, see Figure 58b. This done using the "mesh control" command and setting the edge density to 1mm.	TET10	30mm	3D Tetrahedral mesh.

Table 37: FE analysis no. 9 - Meshing data

Mesh result

Number of elements	Number of nodes
TET10: 51 249	99 723

Table 38: FE analysis no. 9 - Mesh result

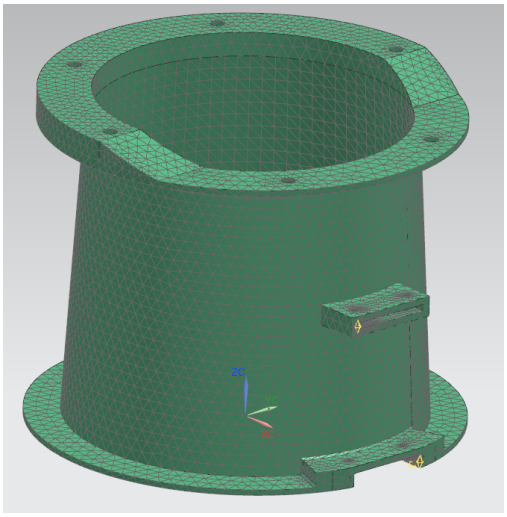

(a) Funnel meshed with TET10 elements.

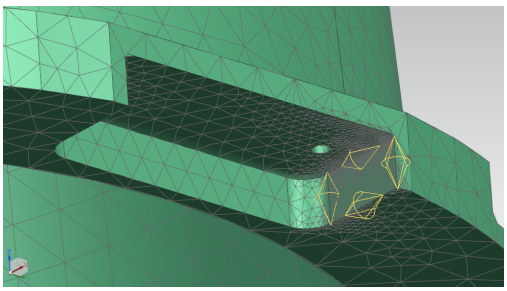

(b) High mesh density at critical area.

Figure 58: Finished mesh of the funnel

Boundary conditions

Before introducing the boundary conditions, the load case needs to be described. The funnel and the anti-rotation pin are not connected to the load case described in section 3.1.2. Due to a an angle misalignment of the XTHT, as figure shows, a rotational motion and torque will occur to the XTHT. The anti-rotation pin which is engaged to the roof, will act as a rotation barrier and create a counter torque. Figure 59 shows rotating motion of the tool and the tilt of the XT due to a angle misalignment. This load case is covered in detail in Appendix E - Angle offset and torque calculations.

The following values is sourced from the mentioned appendix and is based on the requirement of maximum allowed tilt angle of the Xmas Tree (XT) at 1.7°, referring to appendix A - Design basis

- Torque: 41.5 kNm
- Force acting on anti-rotation pin: 83 kN.

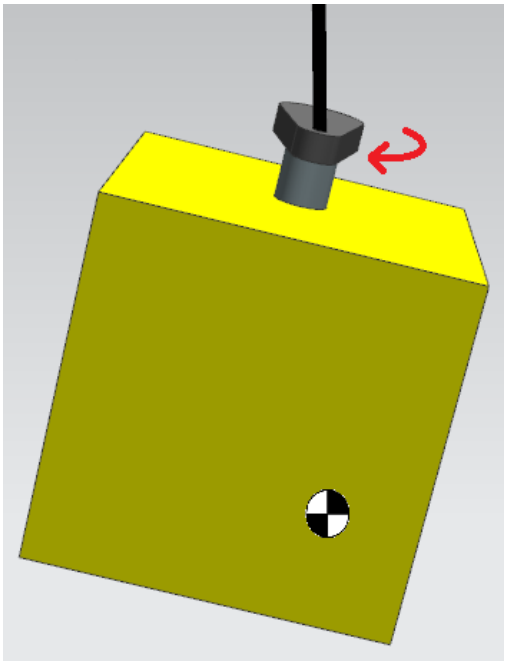

(a) Tool offset

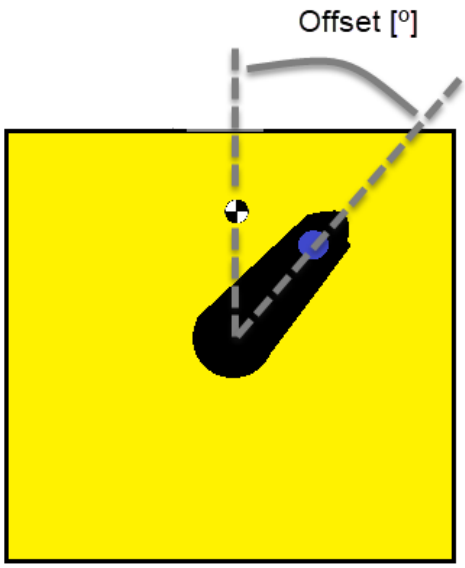

(b) Rotating motion of XTHT as XT tilts.

Figure 59: Rotating motion of the XTHT due to angle misalignment

Its important to mentioned that the friction force in the H4 profile which will act as a counter torque is neglected, and thereby the anti-rotation pin alone which will resist the torque. In other words, this analysis is very conservative and creates a tool which is safe in use. This is done due to the catastrophic consequences that could occur if the XTHT starts rotating at a 70 tonnes heavy XT.

The bracket housings at the funnel (see Figure 57c) take the loads from the anti-rotation pin. The distance from the spool center to the anti-rotation pin is 0.5m, and as shown in Figure 60a, the brackets housing is located at a lower radius. Thereby they experience a higher force. The forces acting in the bracket housing could be find by imagine the anti-rotation pin to be at the bracket housings radius and do an equilibrium calculation. The following equation and figures shows the calculations.

New "Anti-rotation pin force":

$$F = \frac{0.5m * 83kN}{0.429m} = 97kN$$

The following calculations relats to Figure 60b

$$\Sigma M_c = 0 \Downarrow$$

$$F_B * 355mm - 97kN * 455mm = 0 \Rightarrow F_B = \frac{97KN * 455mm}{355mm} = \underline{\underline{124KN}}$$

$$\Sigma F = 0 \Rightarrow F_C = F_B - F_A = 124kN - 97kN = 27KN$$

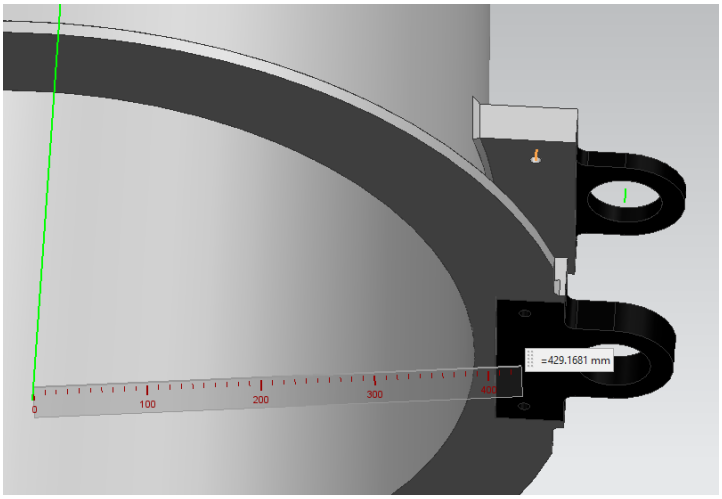

(a) Distance to bracket housing

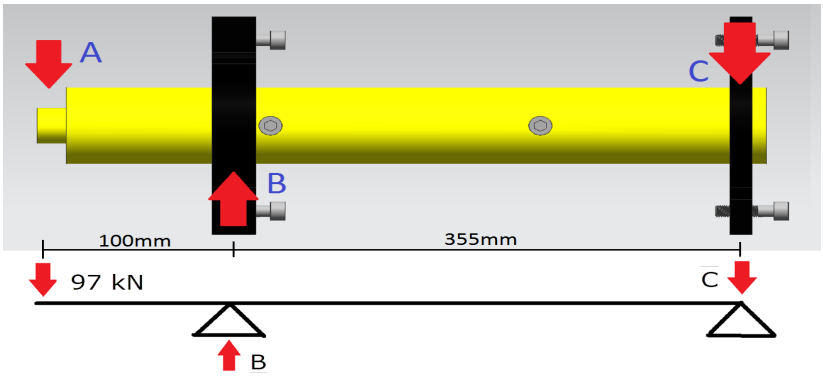

(b) Force B and C corresponds to the forces acting in the bracket housings

Figure 60: Dimensions and forces regarding the funnel bracket housings

Note: The point of the attack of the black brackets is located at 0.5m, while the brackets housings at 0.429m, as Figure 60a shows. This introducing higher pressure to the edge of the bracket housings. As for the locking dogs, a simplification is done, applying an uniform force to the whole bracket housing surface. See the locking dog analysis in section 3.2.5 and its "Boundary conditions" subsection for further details.

Table 39 shows the boundary conditions applied to FE analysis no. 9, while Figure 39 shows the applied boundary conditions.

Boundary conditions

Load			**Fixed constraints/DOF**						
Type	Location	Value	Location	Translation			Rotation		
				X	**Y**	**Z**	**X**	**Y**	**Z**
Force	Lower bracket housing (B).	124kN	The six top holes	√	√				
Force	Upper bracket housing (C).	27kN	Top surface of the funnel			√			

Table 39: FE analysis no. 9 - Boundary conditions

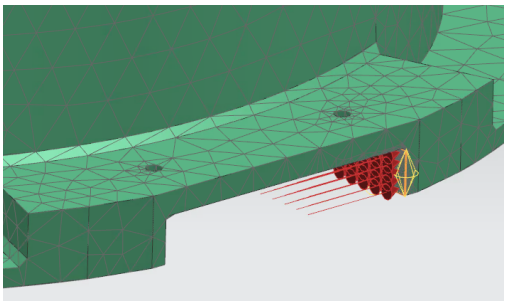

(a) Load applied to lower bracket housing (B).

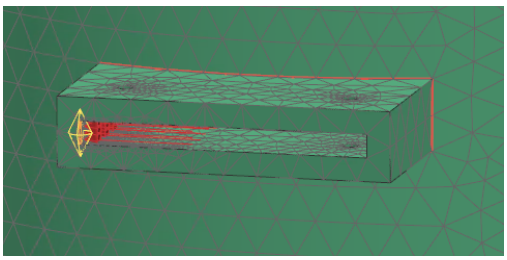

(b) Load applied to upper bracket housing (C).

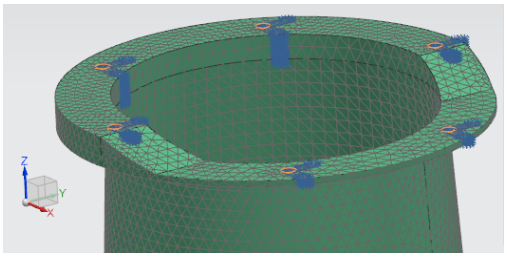

(c) Constrains applied to the six holes

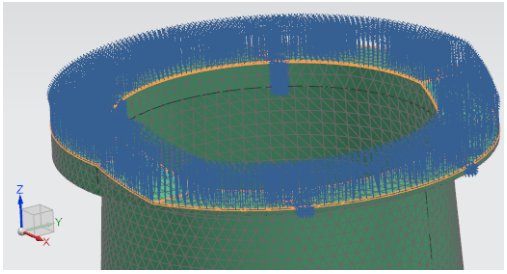

(d) Constrains applied to the top surface of the funnel

Figure 61: FE analysis no. 9 - Boundary conditions at the locking ring.

Results

Table 40 and the following figures provides the results of FE analysis no. 9: Funnel - Anti-rotation pin.

Results

	Value	Unit	Discussion	Conclusion
Maximum stress	**323**	MPa	Figure 62 shows the stress distribution. The highest Von Mises stress is located in the lower bracket housing. The material of the funnel has a yield strength at 355 Mpa, referring to section 3.1.3. Thereby is the stress result is within the requirement.	Approved
Maximum displacement	**0.33**	mm	Figure 63 and figure shows the stress contribution in Y-direction, which is the only relevant direction in the analysis. Figure 61c shows the coordinate system. The highest displacement is located in the lower bracket housing and is considered low and sufficient compared to its adjacent dimensions.	Approved

Table 40: FE analysis no. 9 - Results. Funnel - Anti-rotation pin.

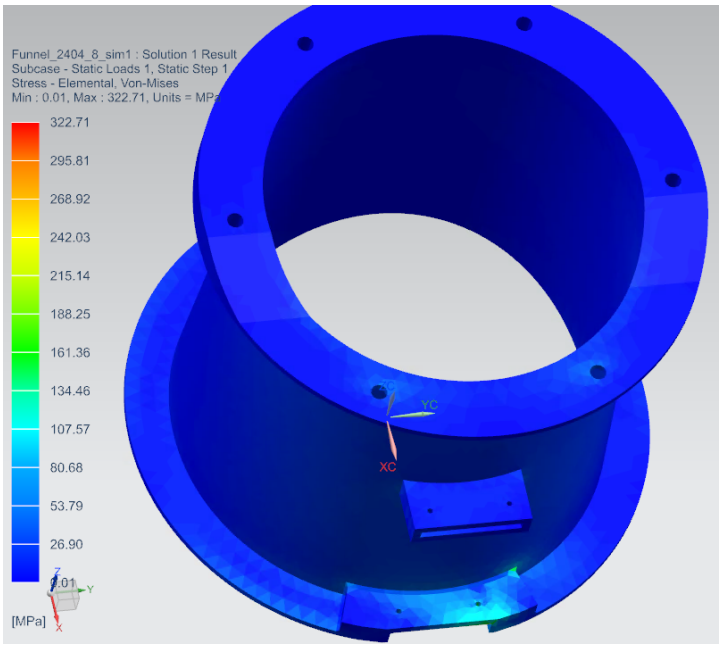

(a) No high stress concentration at the upper part of the funnel.

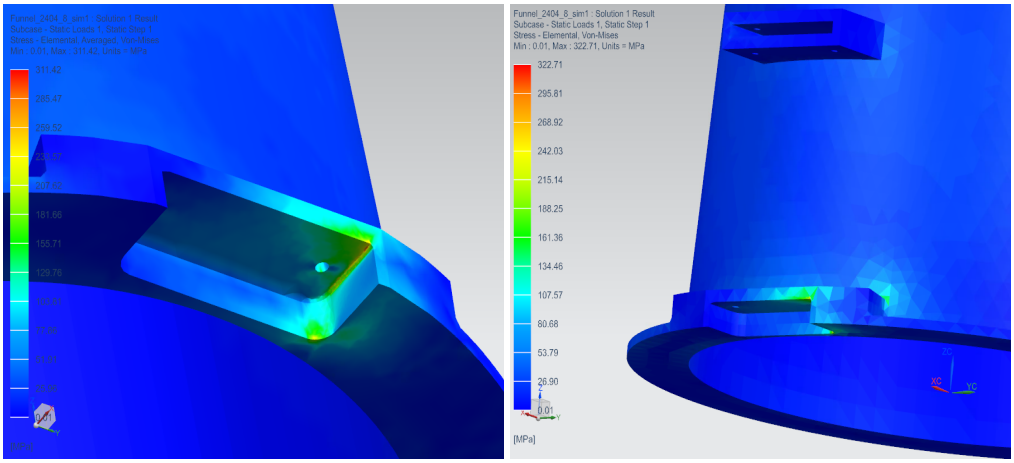

(b) Highest stress in lower bracket housing (c) Upper bracket housing well within the limit

Figure 62: FE analysis no. 9 - Stress result. Funnel - Anti-rotation pin.

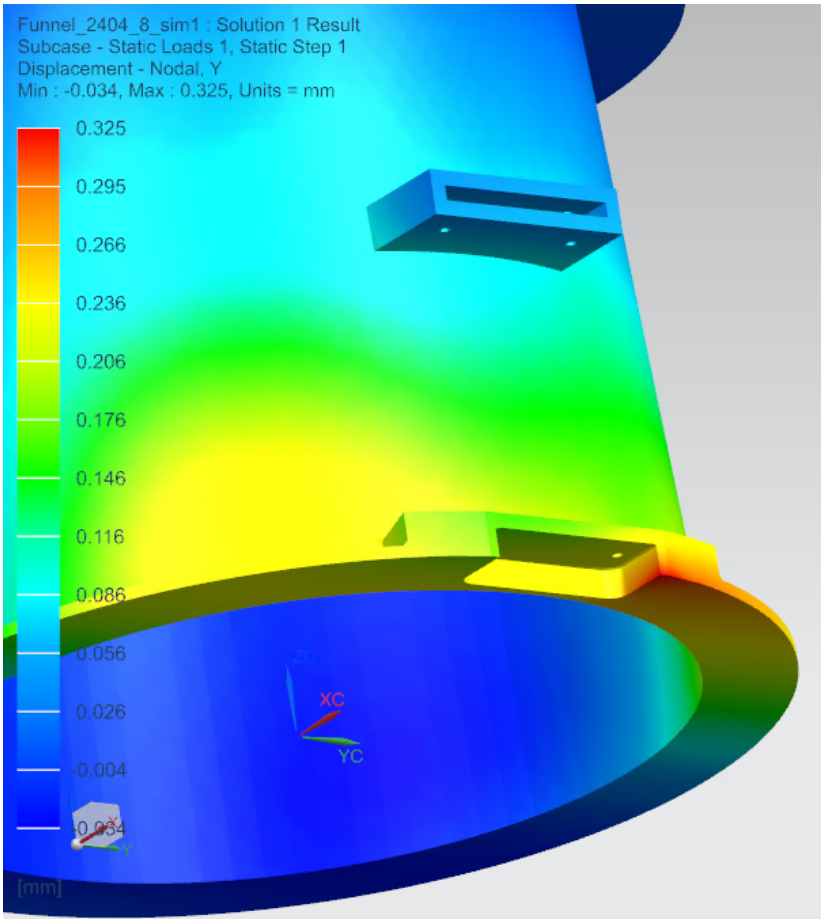

Figure 63: FE analysis no 9. - Displacement results. Funnel - Anti-rotation pin

3.2.11 FE analysis no. 10: End cap - Screw

This analysis covers the end cap, analyzing the load transfer between the screw and the end cap due to a tilted lift.

Geometry

The geometry of the funnel is shown in Figure 64. Figure 64b shows the FE model.

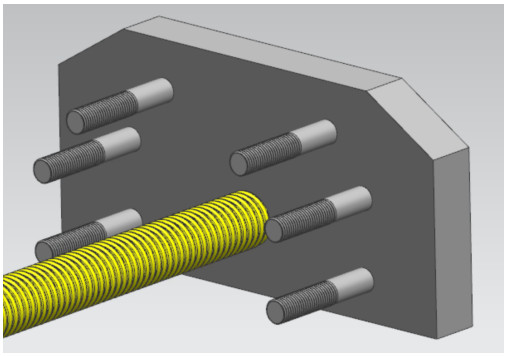

(a) End cap with main screw (yellow) and locking screws

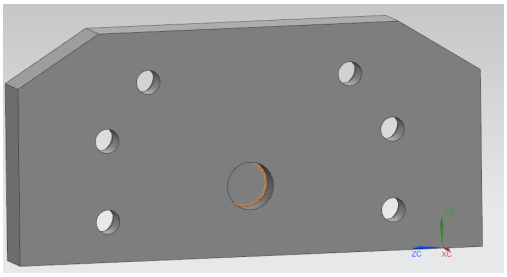

(b) FE model

Figure 64: End cap geometry

Mesh

Table 41 and Table 42 covers the mesh strategy and the mesh result, respectively. The following Figure 65 shows the finished mesh.

Meshing data

Strategy	Element		Features
	Type	Size	
The FE model of the end cap is meshed with TET10 elements. Due to the simple geometry, no special approach or features is necessary..	TET10	10mm	3D Tetrahedral mesh.

Table 41: FE analysis no. 10 - Meshing data

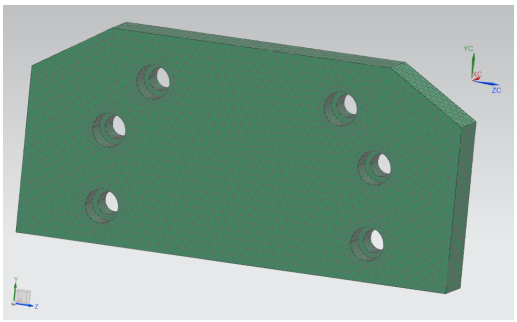

Figure 65: Finished mesh of the end cap.

Mesh result

Number of elements	Number of nodes
TET10: 167 972	260 476

Table 42: FE analysis no. 10 - Mesh result

Boundary conditions

The loads that the end cap will experience is not connected to the load cases described in section 3.1.2 - "Load description". The end cap will experience load as the XT is lifted with a tilt. To get a conservative result, the worst XT tilt angle that possible could occur is used. The screw in the lifting lug needs to withstand the force that goes along the cap, referring to figure. The following calculations and figures shows the resulting XT tilt and forces as the the tool is misaligned with 180°. The dimensions is sourced from appendix A - "Design basis"

XT tilt angle:

$$\alpha = arctan\frac{1m}{2m} = 26^\circ$$

The XT tilt result in the following force acting on the end cap:

$$F = 700kN * \sin 26^\circ = 307N$$

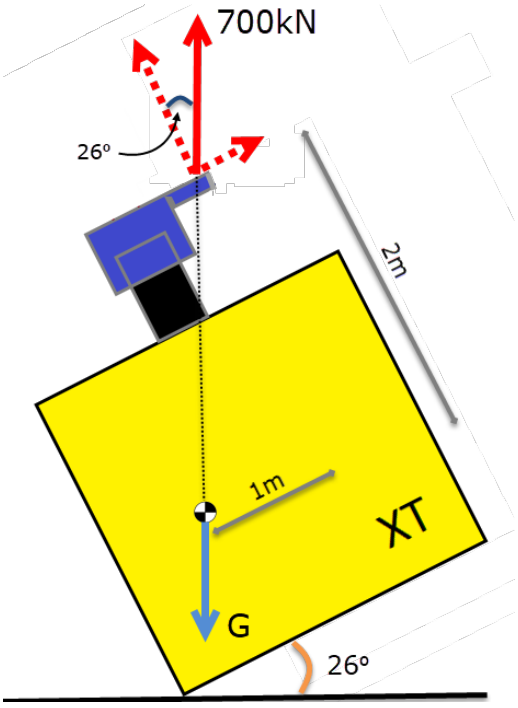

Figure 66: Load scenario as the XT tilts.

Since this is a worst case scenario, a safety factor of two is used instead of four. This conclusion is based on conversations with Aker Solutions, see appendix J - meeting report no.14. This resulting in a force at $F = 2 * 307kN = 614kN$ to be used in the FE analysis.

The boundary conditions is applied in the following way:

- Force at $\frac{614kN}{6} = 102kN$ is applied to each bolt hole, see Figure 67a.
- The bottom of the hole of the yellow screws interface is fixed in X-direction, see Figure 67c.
- The inside of the hole of the yellow screws interface is fixed in Y and Z-direction, see Figure 67d.

- The edge area of the cap is constrained in X-direction, see Figure 67b. . This is done to simulate the support face of the main body, as the these areas will bend if they are not constrained.

The most natural way would have been to applied force at large hole. But its done in the other way around, as constraining the six holes would have created a unnatural high loads at these locations. However, the results would be the same.

Boundary conditions

Load			**Fixed constraints/DOF**						
Type	Location	Value	Location	Translation			Rotation		
				X	**Y**	**Z**	**X**	**Y**	**Z**
Force (Total)	The six small holes	614kN	Large hole, bottom	√					
			Large hole, sidewall		√	√			
			End surface	√					

Table 43: FE analysis no. 10 - Boundary conditions

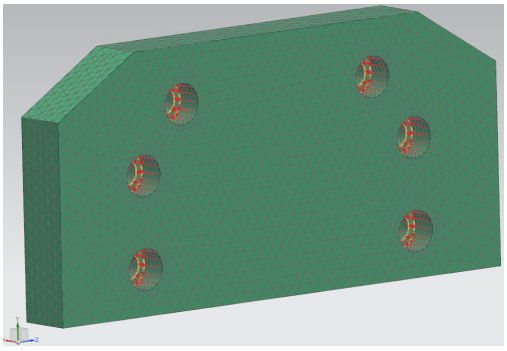

(a) Force applied to the six holes

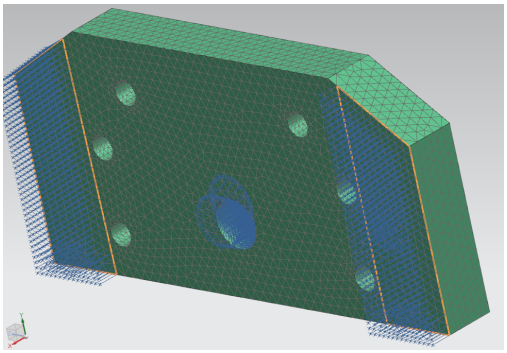

(b) Constrains simulating main body support.

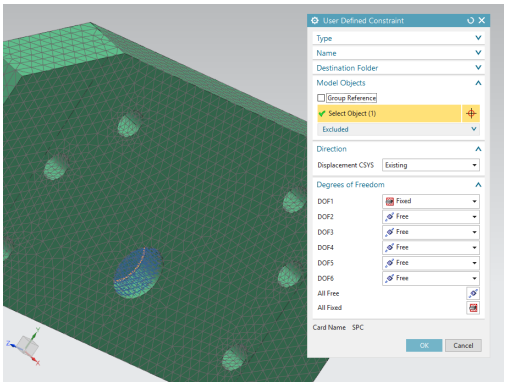

(c) Constraining the main screw hole, bottom.

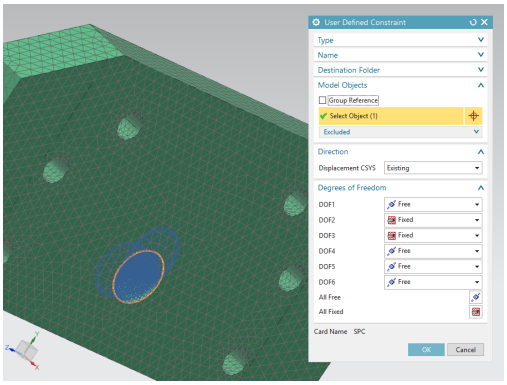

(d) Constraining the main screw hole, sidewall.

Figure 67: FE analysis no. 10 - Boundary conditions at the end cap

Results

Table 44 and the following figures provides the results of FE analysis no. 10: End cap - Screw.

Results

	Value	Unit	Discussion	Conclusion
Maximum stress	**483**	MPa	Figure 68 shows the stress distribution. The highest Von Mises stress is located in main screw hole at 770MPa. As figure shows, this is singularities and could therefore be ignored, as done in previous analysis. The six small holes have some stress concentration, but is not critical and within the requirement at 550 Mpa.	Approved
Maximum displacement	**0.1**	mm	Figure 69 shows the stress contribution in X-direction, which is the only relevant direction in the analysis. The highest displacement is located at the middle of the cap as expected, and bracket is considered low and sufficient compared to its adjacent dimensions.	Approved

Table 44: FE analysis no. 10 - Results. End cap - Screw.

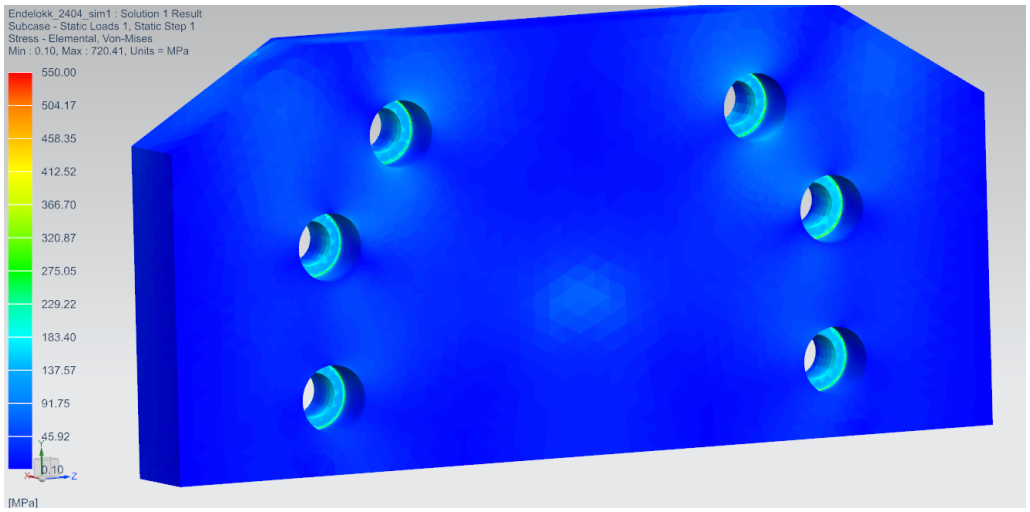

(a) Front view

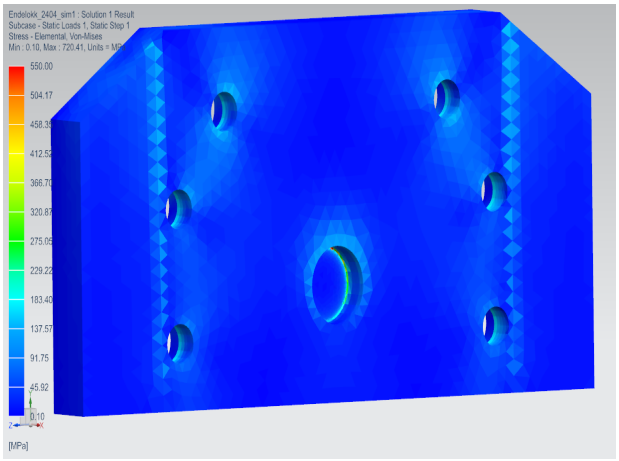

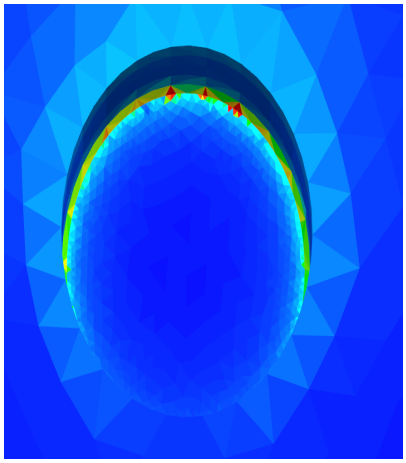

(b) Back view (c) Singularities in the large hole

Figure 68: FE analysis no. 10 - Stress result. Funnel - End cap - Screw.

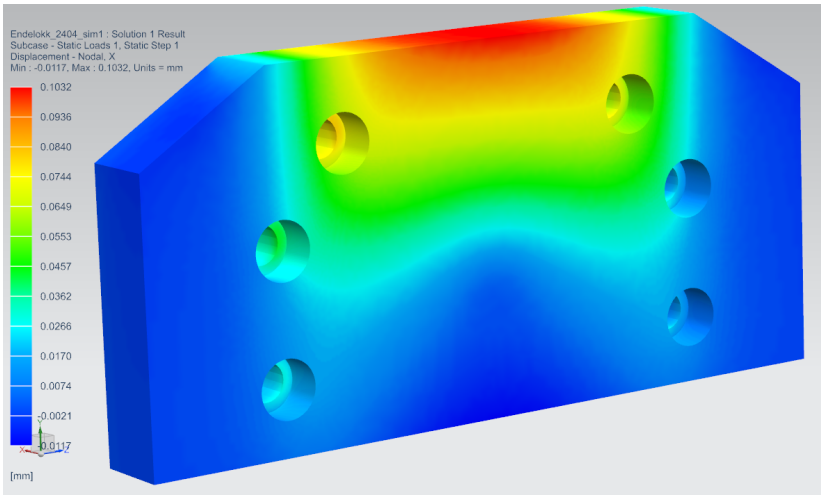

Figure 69: FE analysis no 10. - Displacement results. End cap - Screw

3.3 Hand calculations

3.3.1 Screw

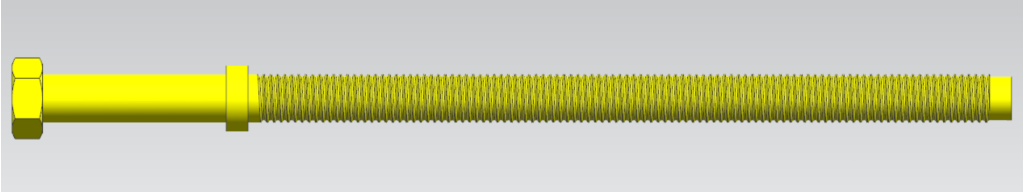

Figure 70: Screw

The screws purpose is to adjust the lifting lug to the desired radius. During a tilted lift, the screw prevents the lifting lug from sliding and needs to withstand these forces. This load case, safety factor and worst tilt scenario is covered in section 3.2.11 - "FE analysis no. 10: End cap - Screw".

The thread size needs to be calculated. This is done by solving the minimum screw cross section, which is as follows:

$$A = \frac{F * SafetyFactor}{\sigma} = \frac{307KN * 2}{355MPa} = 1730mm^2$$

The chosen screw size is a standard M56, with a sufficient cross section of 2030mm^2.

Note: If the XT tilt the other way, the main body would have to encounter the force instead of the end cap. The worst case scenario is at 14°, as the lifting lug i positioned in center(0.5m offset from COG). This result in a much lower force acting in the main body, and thereby is this scenario considered as sufficient without any special calculations.

Screw Bearing Stress

The screws supported in both ends with no roller/ball bearing. If the XT is lifted with a tilt, the lifting lug would try to slide while the screw prevents it from happening. When the screw is pushed axially, the surface pressure cannot exceed the yield strength. Minimum area is for the lid is 1730mm^2 as calculated above.

The minimum needed area that touches the body is

$$A = \frac{F * SafetyFactor}{\sigma} = \frac{700KN * sin14 * 2}{355MPa} = 954mm^2$$

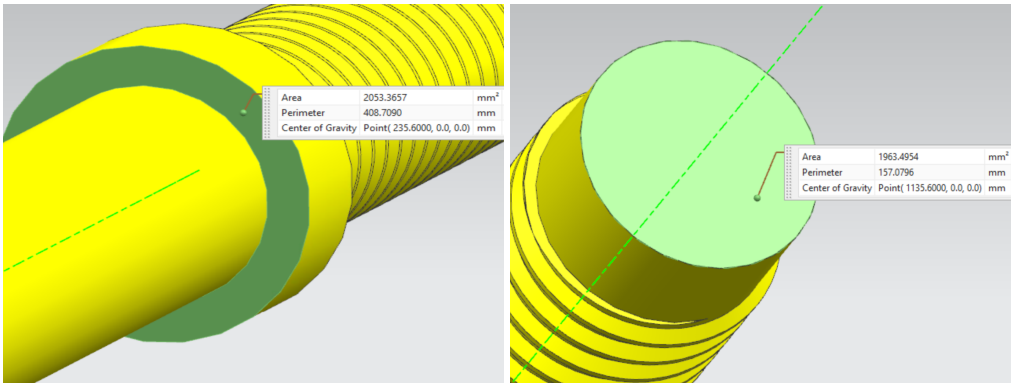

(a) The area that touches the body(2053mm^2) (b) The area that touches the end cap(1963mm^2)

Figure 71: Worst case bearing stress

As the Figure 71 shows, both surface areas is larger than the required surface.

3.3.2 End cap bolts

The bolts that connects the end cap to the main body need to withstand the loads generated during a tilted lift of the XT. This load case, safety factor and worst tilt scenario is covered in section 3.2.11 - "FE analysis no. 10: End cap - Screw". The minimum screw cross section of one single bolt is calculated as follows:

$$A = \frac{F * SafetyFactor}{\sigma * NumberOfScrews} = \frac{307KN * 2}{355MPa * 6} = 288mm^2$$

The chosen screw size is a standard M24, with a sufficient cross section of 358mm^2

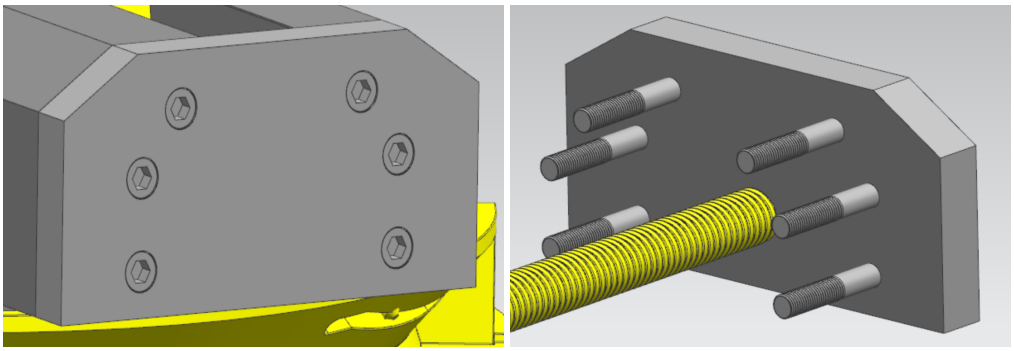

(a) Six screws holding the lid (b) Inside view

Figure 72: End Cap

3.3.3 Anti-rotation parts

To prevent the XTHT from rotating on the spool due to a misaligned tool, the anti-rotation pin penetrates a hole in the roof and withstands the torque. The pin is connected to the funnel, which is calculated in section 3.2.10. The anti rotation pin and its brackets, are calculated by hand in this section.

The force acting on the pin would be 20.7kN when the XT is lifted with a 1.7 degrees tilt, referring to appendix E. With 4 in safety factor, the design force would be 83kN. Forces

acting on the pin and dimensions are shown in Figure 73.

Roof

It is assumed that the roof is strong enough to encounter such loads. However, hole pressure stress neeeds to be calculated. The minimum roof thickness is calculated as follows:

$$\frac{F}{\sigma * diameter} = t$$

$$\frac{83KN}{355MPa * 30mm} = 7.79mm$$

Typical roof thickness is at 16mm, and thereby hole pressure within the requirement. Roof thickness at 16mm is based on a dimension study including the following projects (see bibliography for sources):

- Aerfugl 7X5 VXT [4]
- Aastad Hansen 7X5 HXT [5]
- Dvalin 7X5 HXT [6]
- Troll phase 3 7x7 VXT [7]

Locking pin

To find the loads which the pin is exposed to, an equilibrium calculation is performed. The following formulas reflects the calculations, while relating to Figure 73.

$$\Sigma M_c = 0$$

$$F_B = \frac{83KN * 455mm}{355mm} = 106KN$$

$$F_C = F_B - F_A = 106KN - 83KN = 23KN$$

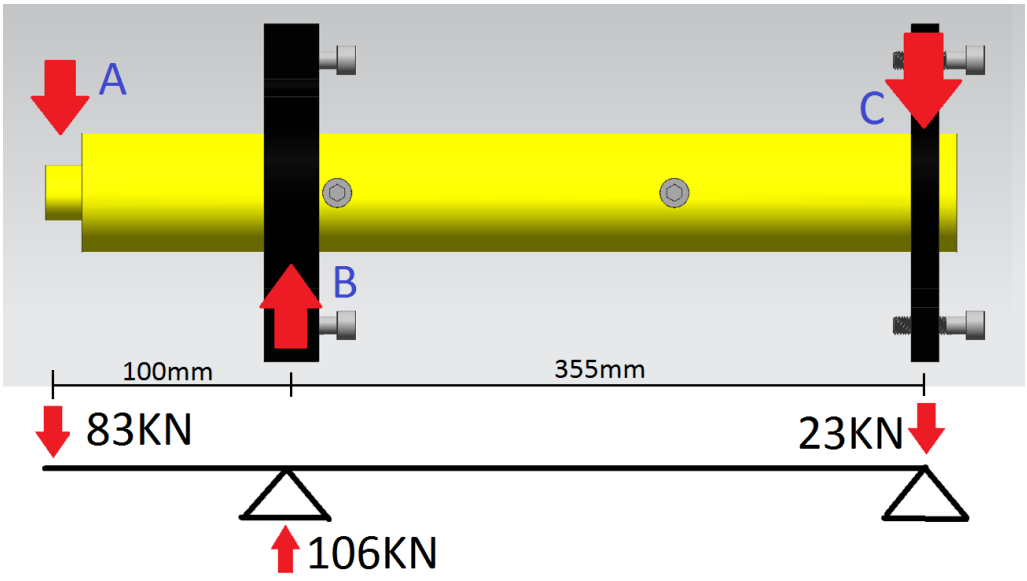

Figure 73: Force acting on the pin, yellow pin and black brackets

The locking pin needs to withstand shear- and bending stress. A pin diameter of 65mm is selected for the main cylinder and 30mm is chosen for the tip. First bending stress is calculated as follows:

$$\sigma_{bend} = \frac{M_b}{W} = \frac{F * arm * 32}{\pi * D^3} = \frac{83KN * 100mm * 32}{\pi * 65mm^3} = 307MPa$$

Shear stress is calculated as follows:

$$\tau = \frac{4 * F}{\pi * d^2} = \frac{4 * 83KN}{\pi * 65^2} = 25MPa$$

The total stress the pin experience can be calculated with Von Mises yield criterion, which combines shear and bending stress. The total stress cannot exceed the yield strength of the material at 355MPa.

$$\sigma_{vm} = \sqrt{\sigma_b^2 + 3 * \tau^2} = \sqrt{307MPa^2 + 3 * 25MPa^2} = 310MPa < 355MPa$$

This confirms the pin diameter of 65mm to be sufficient.

The thin tip at 30mm in diameter, will only experience pure shear stress and no bending. The shear stress needs to be below 205MPa.

$$\frac{355MPa}{\sqrt{3}} = 205MPa$$

$$\tau = \frac{4 * F}{\pi * d^2} = \frac{4 * 83KN}{\pi * 30^2} = 117MPa < 205MPa$$

The results confirms sufficient strength of the tip.

Top locking pin bracket

These brackets needs to be solid enough to handle every kind of load the pin is exposed to. Assume 15mm thickness of bracket and 20mm material around the hole, referring to Figure 74a for illustration. The following formulas calculates the "Tear out stress", "Rupture stress" and "Bearing stress" and relates to Figure 74a.

$$\tau_{TearOut} = \frac{F}{A} = \frac{23KN}{20mm * 15mm * 2} = 38MPa < 205MPa$$

$$\sigma_{Rupture} = \frac{F}{A} = \frac{23KN}{20mm * 15mm * 2} = 38MPa < 355MPa$$

$$\sigma_{BearingStress} = \frac{F}{Thickness * Diameter} = \frac{23KN}{15mm * 65mm} = 24MPa < 355MPa$$

Bottom locking pin bracket

The bottom bracket has the same dimensions as the top bracket, except a thickness of 30mm and a force of 106KN. The results are as follows:

$$\tau_{TearOut} = 118MPa < 205MPa$$

$$\sigma_{Rupture} = 118MPa < 355MPa$$

$$\sigma_{BearingStress} = 109MPa < 355MPa$$

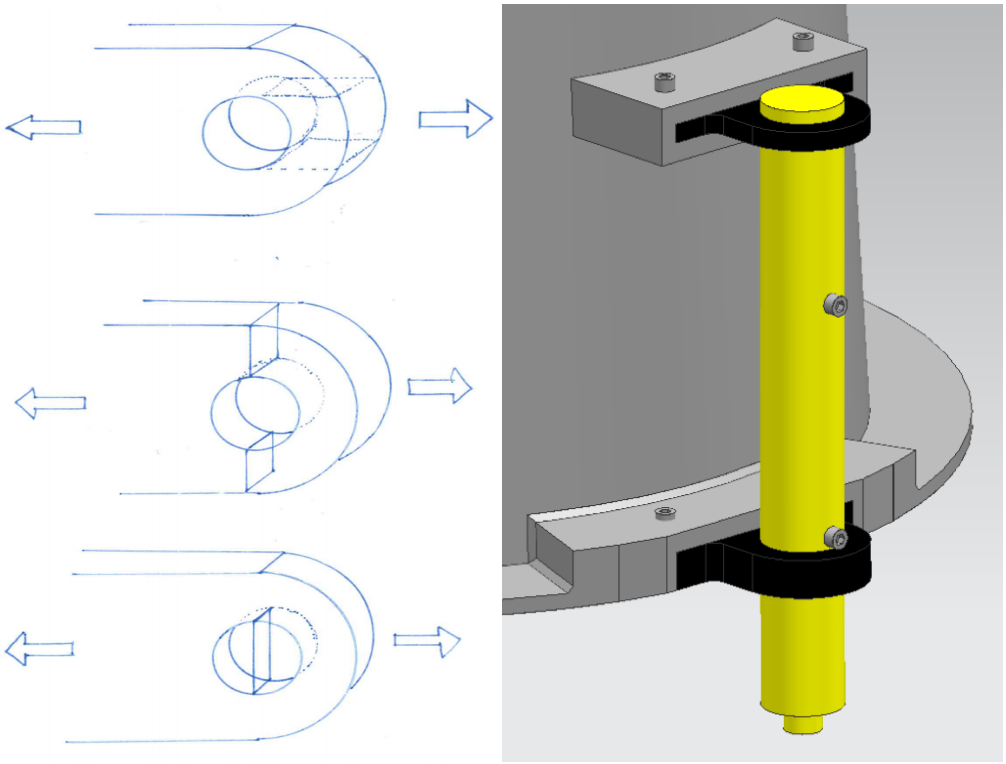

(a) Tear-out-, rupture- and bearing stress (b) Mounted on funnel, fully extended

Figure 74

3.3.4 Transmission pin

The pins that moves and holds the straight dogs in place is exposed to a lot of pressure when lifting. When friction between the dogs and body is neglected, the pin is exposed to 460KN axial force, referring to section 3.2.9. Material that is being used has a yield tension of 550 MPa, referring to section 3.1.3.

The minimum area needed to be within the requirement is as follows:

$$Area = \frac{F}{\sigma} = \frac{460KN}{550MPa} = 836mm^2$$

There are two critical areas that need to be considered.

- **First area, referring to Figure 75a**
  Section view in the middle of the transmission pin. Total area of $1860mm^2$ and thereby sufficient.
- **First area, referring to Figure 75b**
  Interface to straight locking dog. Total area of $1188mm^2$ and thereby sufficient.

Figure 75a shows a section view in the middle and 75b shows the areas. Th The area of both sides of the transmission pin Figure 75a and the area between the pin and the dog Figure 75b. They are both OK.

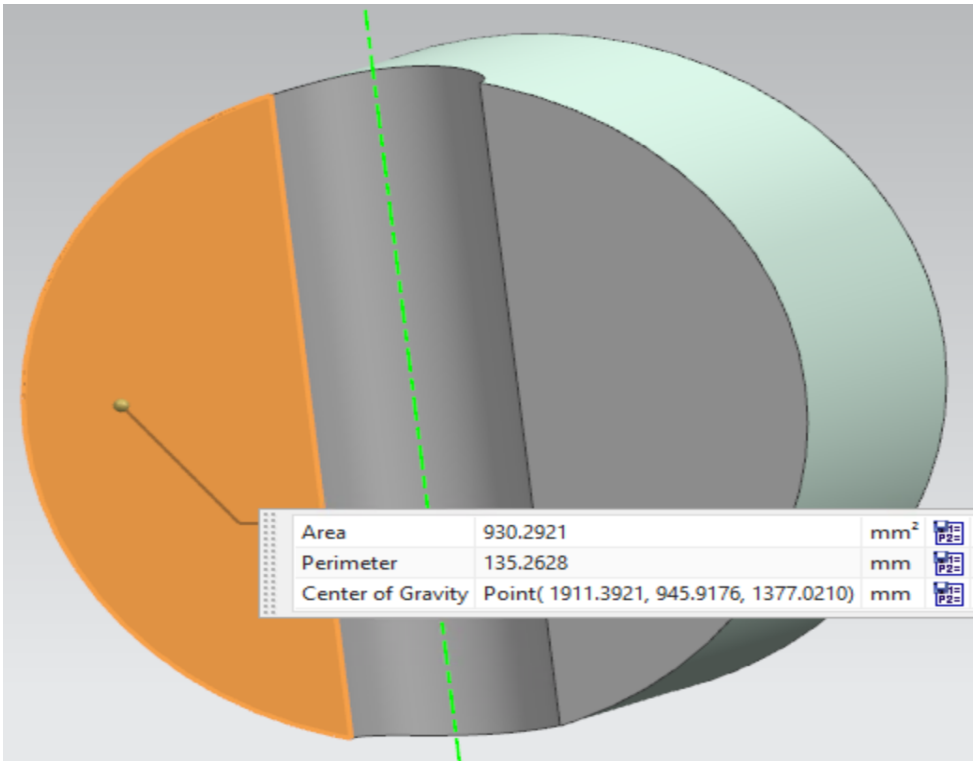

(a) First area

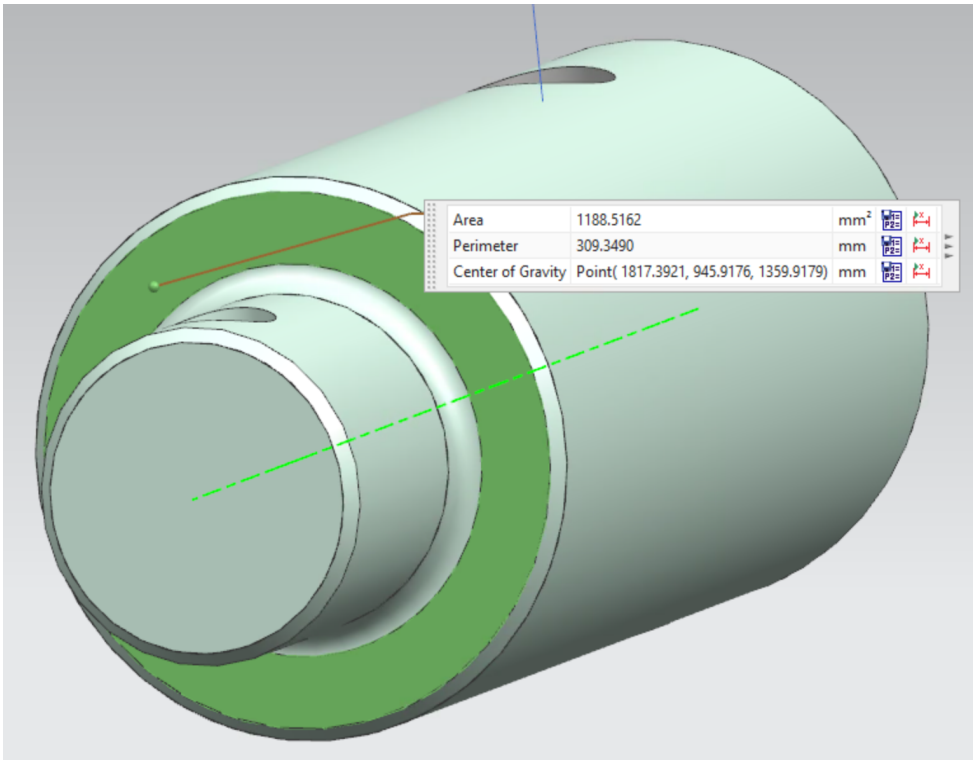

(b) Second area

Figure 75: Transmission pin and critical areas

4 Results

This chapter summarizes all the results of the calculation report, see table 45 and 46.

FE Analysis results

No.	Description	Maximum stress[MPa]	Maximum displacement[mm]
1	Lifting lug - Main body	541 < 550	0.2
2	Main body - Lifting lug. Off-center lift	466 < 550	0.53
3	Main body - Lifting lug. Center lift	290 < 550	0.3
4	Main body - Locking dogs. Off-center lift	489 < 550	0.51
5	Main body - Locking dogs. Center lift	348 < 550	0.25
6	Locking dog - Main body. Straight dog	197 < 550	0.03
7	Locking dog - Main body. Tilted dog	371 < 550	0.13
8	Locking ring - Transmission pin	680 > 550	0.93
9	Funnel - Anti-rotation pin	323 < 355	0.33
10	End cap - Screw	483 < 550	0.1

Table 45: Overview of the results - FE Analysis

Hand calculations results

Description	Acceptance / Result
Screw: Minimum cross section / Current cross section	$1730mm^2$ / $2030mm^2$
End cap bolts: Minimum cross section / Current cross section	$288mm^2$ / $358mm^2$
Roof: Minimum thickness / Typical thickness	$7.8mm$ / $16mm$
Anti-rotation pin: Maximum accepted stress / Von Mises stress Maximum accepted stress / Pure shear stress	 355 MPa / 310 MPa 355 MPa / 117 MPa
Anti-rotation bracket, upper: Maximum accepted stress / Tear out stress Maximum accepted stress / Rapture stress Maximum accepted stress / Bearing stress	 205 MPa / 38MPa 355 MPa / 38Mpa 355 MPa / 24MPa
Anti-rotation bracket, lower: Maximum accepted stress / Tear out stress Maximum accepted stress / Rapture stress Maximum accepted stress / Bearing stress	 205 MPa / 118MPa 355 MPa / 118MPa 355 MPa / 109MPa
Transmission pin: Minimum cross section / Current cross section	$836mm^2$ / $1188mm^2$

Table 46: Overview of results - Hand calculations

5 Discussion

The calculation report reflects many analyses and calculations. Therefore, each calculation have been discussed continuously throughout the report. This chapter discusses some common and general aspects of the report, as well as listing some potential improvements.

In every analysis and calculations, the intention and objective has been to verify structural integrity of the XTHT. Every component were within the requirements and concluded to have sufficient strength for the applicable load case, except from FE analysis no.6 were computing problems occurred.

The calculation report proves that is possible to make a tool which could lift in a off-center position. But due to the level of skill which the students possess in Finite Element Analysis (FEA), the analysis needs be considered as a first revision of a finished calculation report. The analyzes needs to be verifies by professionals before the 70 tonnes lifting capacity can be finally confirmed, as well as reproduce FE analysis no.6 and approve this.

Note: There has not been done mesh convergence studies in any of the analysis. A fine mesh has been applied to critical areas, but due to lack of time, no convergence study has been conducted.

5.1 Potential improvements

This section covers a list of potential improvements that could be done before a possible implementation.

- **Contact simulation in FEA**
  A contact simulation would probably give more precise results.
- **FEA of the roof**
  In this report it is assumed that the roof is strong enough to encounter the applied force. This needs to be studied.
- **Mesh convergence study**
- **Optimize corners**
  Fine tune corners in terms of stress concentration.
- **Weight optimization**
  Most of the parts is weight optimized, but there are some parts that could use further improvements.
  - **Main body**
    Thickness close to the lifting lug could have been reduced. Also the thickness of the housing around the spool could have been reduced, especially on the "A-side".
  - **Dogs**
    The dogs could have been shallower. Which result in a slimmer main body.
  - **Locking ring**
    It can be optimized since there is a person that is supposed to rotate the ring.
  - **Funnel**
  - **End cap**
    The six mounting screws can be reduced in size or number.

- **Improve in terms of production/machining**
  When optimizing the tool in terms of strength, keep in mind to optimize for easier/cheaper production.

6 Conclusion

The XTHT is concluded to have sufficient strength to perform its intended lifting operations, both in a center and off-center position. Off-center lifting introduced high loads and tensions to the tool, but the results was still within the acceptance criteria. The analysis needs to be verified by professionals before the 70 tonnes lifting capacity can be confirmed. In addition to that, a list is made to itemize potential improvements that could be conducted before a possible implementation.

Bibliography

[1] Siemens. Siemens website. https://www.plm.automation.siemens.com. (Visited Feb. 2019).

[2] Harald Falck-Ytter. *Materialteknologi, Del 1 Grunnlag*. Gyldendal, 1984.

[3] Aker Solutions. Calculation report, xtht. Internal, 2014. DIR: 10000233693.

[4] Aker Solutions. Drawing of roof, aerfugl 7x5 vxt. Internal, 2018. DIR: 10003585025.

[5] Aker Solutions. Drawing of roof, aastad hansen 7x5 hxt. Internal, 2014. DIR: 10002046166.

[6] Aker Solutions. Drawing of roof, dvalin 7x5 hxt. Internal, 2014. DIR: 10002346411.

[7] Aker Solutions. Drawing of roof, troll phase 3 7x7 vxt. Internal, 2019. DIR: 10003726971.